TECHNICAL REPORT ARBRL-TR-02365

DESIGN OF KINETIC ENERGY PROJECTILES FOR STRUCTURAL INTEGRITY

W. H. Drysdale

September 1981

US ARMY ARMAMENT RESEARCH AND DEVELOPMENT COMMAND
BALLISTIC RESEARCH LABORATORY
ABERDEEN PROVING GROUND, MARYLAND

Destroy this report when it is no longer needed.
Do not return it to the originator.

Secondary distribution of this report by originating or sponsoring activity is prohibited.

Additional copies of this report may be obtained from the National Technical Information Service, U.S. Department of Commerce, Springfield, Virginia 22151.

The findings in this report are not to be construed as an official Department of the Army position, unless so designated by other authorized documents.

The use of trade names or manufacturers' names in this report does not constitute indorsement of any commercial product.

UNCLASSIFIED
SECURITY CLASSIFICATION OF THIS PAGE (When Data Entered)

REPORT DOCUMENTATION PAGE

READ INSTRUCTIONS BEFORE COMPLETING FORM

1. REPORT NUMBER (15) TECHNICAL REPORT ARBRL-TR-02365
2. GOVT ACCESSION NO. AD-A105 502
3. RECIPIENT'S CATALOG NUMBER

4. TITLE (and Subtitle) (6) DESIGN OF KINETIC ENERGY PROJECTILES FOR STRUCTURAL INTEGRITY
5. TYPE OF REPORT & PERIOD COVERED (9) Technical Report
6. PERFORMING ORG. REPORT NUMBER

7. AUTHOR(s) (10) W. H. DRYSDALE
8. CONTRACT OR GRANT NUMBER(s)

9. PERFORMING ORGANIZATION NAME AND ADDRESS
U.S. Army Ballistic Research Laboratory
ATTN: DRDAR-BLI
Aberdeen Proving Ground, MD 21005
10. PROGRAM ELEMENT, PROJECT, TASK AREA & WORK UNIT NUMBERS (11) 1L662618AH80

11. CONTROLLING OFFICE NAME AND ADDRESS
U.S. Army Armament Research & Development Command
U.S. Army Ballistic Research Laboratory
ATTN: DRDAR-BL
Aberdeen Proving Ground, MD 21005
12. REPORT DATE SEPT [redacted] 81
13. NUMBER OF PAGES (12) 60

14. MONITORING AGENCY NAME & ADDRESS (if different from Controlling Office)
15. SECURITY CLASS. (of this report) UNCLASSIFIED
15a. DECLASSIFICATION/DOWNGRADING SCHEDULE

16. DISTRIBUTION STATEMENT (of this Report)
Approved for public release; distribution unlimited

17. DISTRIBUTION STATEMENT (of the abstract entered in Block 20, if different from Report)

18. SUPPLEMENTARY NOTES

19. KEY WORDS (Continue on reverse side if necessary and identify by block number)
Kinetic Energy Projectiles
Structural Design
Structural Integrity
Strength of Materials

20. ABSTRACT (Continue on reverse side if necessary and identify by block number) jmk

In this report, rational design of long-rod kinetic energy projectiles is considered from the aspect of structural integrity. Primary emphasis is placed on determining the length and configuration of a sabot which is capable of supporting the subprojectile during launch. Strength of materials methods are utilized for the initial design steps; subsequently, finite element techniques are introduced to obtain improved assessments of the total projectile structural integrity. A simplified rule to estimate sabot mass is developed as part of the analysis.

DD FORM 1 JAN 73 1473 EDITION OF 1 NOV 65 IS OBSOLETE

UNCLASSIFIED
SECURITY CLASSIFICATION OF THIS PAGE (When Data Entered)

1 of 3471

TABLE OF CONTENTS

LIST OF ILLUSTRATIONS

I. INTRODUCTION

The modern development of antiarmor kinetic energy projectiles has been in the direction of long-rod, fin stabilized penetrators. This configuration, while extremely lethal at the target, is fragile during the interior ballistic phase of flight. A great deal of design effort must be expended to ensure launchability of the projectile, i.e. in-bore structural integrity. Since the subprojectile is typically cradled within a multisegmented sabot during this portion of travel, the problem effectively centers on the development of adequate sabot design principles.

Besides ensuring launchability, a sabot is intended to improve the performance of a projectile in terms of either higher velocity or extended range. This improvement occurs because the bore area on which the gun pressure acts may be greatly increased with only relatively modest increases in total projectile launch weight, leading to significantly enhanced acceleration. Obviously, to obtain the optimum performance improvement, the sabot mass must be kept as low as possible within the constraints set by the in-bore structural requirements of the projectile.

These requirements are[1]

- The bore of the gun must be sealed against the hot, high-pressure propellant gas
- The subprojectile must be supported during in-bore travel so that unwanted permanent deformations or fractures do not occur
- The force applied to the sabot by the propellant gas pressure must be transferred across the sabot/subprojectile interface for the acceleration of the subprojectile.

In addition to these primary structural integrity requirements, the proper functioning of the subprojectile requires that the sabot constrain the balloting motion of the projectile during in-bore travel and, subsequently, discard at the muzzle in such a manner as to impart low yaw and yaw rate to the flight body. These latter requirements may be related to target dispersion and for this reason must be minimized. Minimizing yaw and yaw rate demands the solution of a complicated problem in analytical dynamics. Facets of the required analysis include the location of the projectile centering band relative to the center of gravity, the location and stiffness of additional boreriding supports, and the bending modes of the accelerating projectile, coupled with the vibratory motion of the gun barrel and aerodynamic forces at muzzle exit. These dynamic design requirements of the projectile will not be addressed in this report so

[1] *Sabot Technology Engineering, Engineering Design Handbook, AMC Phamphlet 706-445, Department of Army, Washington, DC, July 1972.*

that structural integrity may be emphasized. In any event, at the present moment there is no coherent analysis and design methodology to address these additional sabot requirements.

The basic flight configuration of the subprojectile is assumed to be specified by terminal ballistic and aerodynamic considerations. Thus the length to diameter ratio, diameter, material of the penetrator, and the fin and nose cone weight may not be altered to any significant extent by the projectile designer.

As mentioned, the structural integrity of the total projectile during launch may be effectively reduced to the adequacy of the design principles invoked for the sabot. This does not mean that the design of the sabot may be divorced from the mechanical behavior of the subprojectile. All viable analysis or design methodologies must consider the sabot/penetrator as an integrated system. The payoff for this added complexity is the potential for significant improvements in the performance of kinetic energy projectiles due to the increased structural efficiencies. The present report outlines a rational design procedure to achieve this goal.

II. PRELIMINARY CONSIDERATIONS

A. Projectile Loading

The projectile must be designed to survive the most severe loading conditions it is likely to experience. Since the major forces acting during the interior ballistic cycle are the propellant gas pressure and the resultant inertial body forces, the design condition occurs at the point of maximum pressure. Maximum pressure in a tank gun system, as may be seen from typical pressure-time data, occurs a few milliseconds after propellant ignition, when the projectile has already begun to move within the barrel. The influence of temperature coefficient on burning rate of solid propellant grains causes this maximum pressure to be dependent on the ambient temperature of the propellant. The highest pressure is encountered at the highest temperature, which, for design and testing purposes, has been arbitrarily specified as 63°C (145°F). In a well designed system, this maximum pressure is approximately equal to the allowable tube pressure determined by the designs of the gun/breech combination from fatigue, fracture, or erosion considerations.

The maximum gas pressure occurs in the chamber of the gun. The projectile does not actually experience this pressure, since it has begun to move down tube by this time on the pressure-time curve. The inertial effects of the propellant grains and combustion gases moving out of the chamber, into the barrel, result in a damping of the maximum pressure acting on the base of the projectile. An estimate of the pressure "seen" by the projectile is obtained from the Lagrange correction[2].

[2] *Interior Ballistics of Guns, Engineering Design Handbook, AMC Phamphlet 706-150, Department of Army, Washington, DC, February 1965.*

To derive this necessary formula one assumes that one half of the total charge mass moves down the barrel with the same acceleration as the projectile. (This means that the mass of propulsion products following the projectile neither lags behind nor overtakes the projectile). Thus, at the mouth of the chamber

$$P_C A_B = (M + \tfrac{1}{2} C) \ddot{Z} , \qquad (1)$$

where

P_C = chamber pressure,

A_B = bore area of gun tube,

M = total projectile mass,

C = propellant mass, and

$\ddot{Z}$ = axial acceleration of projectile and propellant.

The acceleration of the projectile may also be written by considering the (reduced) pressure acting on the projectile.

$$\ddot{Z} = \frac{P_B A_B}{M} , \qquad (2)$$

where

P_B = base pressure on projectile.

Substituting Eq. (2) into Eq. (1) and solving for P_B yields the Lagrange correction to base pressure

$$P_B = \frac{P_C}{1 + \frac{C}{2M}} . \qquad (3)$$

The time of interest is at the time of peak pressure. Thus, for tank gun application, where the charge to mass ratio is approximately one this correction is respectably accurate and generally conservative when compared to the existing experimental data. The effective base pressure acting on the kinetic energy tank projectile is thus typically only 2/3 of the maximum chamber pressure. Ignoring this reduction leads to overly conservative design requirements.

The other major load applied to the projectile during peak loading is the inertial body force. The base pressure applied to the sabot will generate an axial acceleration of an often impressive magnitude. For dense penetrator materials, this body force is the primary load which effectively drives the design. When bore friction is ignored (a conservative simplification) the axial accelerations may be found from Eq. (2) as soon as the projectile mass and base pressure are known.

At the entrance to the barrel of the gun, the obturating or rotating band is pressed through a forcing cone, placing this band under high compressive stresses. In addition a rifled gun tube will also engrave the band. Pressure is transmitted to the band seat; this load remains relatively constant for the entire in-bore travel of the projectile. (The wear of the band material from rubbing against the bore, especially at high velocity, will reduce the compression somewhat by muzzle exit). The magnitude of the band pressure may theoretically be calculated, since the initial band shape and the geometry of the forcing cone and band seat are known. In practice this calculation is very difficult. The large compression ratio used to ensure a tight seal for the high pressure propellant gas means that the deformation is nonlinear, both in terms of large strain and plastic flow. Modern obturating bands are typically made of polymeric materials because of low bore friction, reduced muzzle wear, and good pressure sealing experience. Unfortunately, the constitutive relations for these materials are highly temperature and rate of loading dependent, especially under plastic flow conditions. Additional loadings are superimposed on this gross compression, e.g. sliding friction against the bore of the gun base pressure over portions of the rear face of the band, acceleration inertial forces, reactions of the elastic band seat material, and, for the case of rifled gun tubes, torque due to the rifling, and slip surfaces on the band seat (for despinning the projectile). Extremely advanced numerical techniques, such as the incremental finite element method, are required to even approximately model this complicated behavior in a rational manner. For this reason, band and band seat designs remain an empirical science beyond the scope of this report. Estimates of band pressure for projectile design efforts are generally obtained experimentally from a similar configuration, either from instrumented gun tube firings or static shell pusher tests[3].

A final potential source of projectile loading during the time of peak pressure may be obtained from analysis of the dynamical motion of the projectile. The determination of the magnitude and points of application of the in-bore transverse loads is effectively an unsolved

[3] *John M. Hurban and Stephen G. Sawyer, "Analysis of Effective Band Pressure in the 152 mm Gun Tube Using Finite Elements and Shell Pushing Data", Proceedings of U.S. Army Science Conf., West Point, NY, June 1972.*

problem at the present, although see reference 4. These tranverse loads are the constraint forces required to maintain the moving projectile within the bore surfaces of the vibrating and translating gun tube, with the maximum permissible yawing motion determined by projectile/bore clearances. These forces may be applied impulsively as well as randomly since innumerable perturbations of conditions may occur, for example turbulant flow of the propellant gas over fins. The requirement for the projectile designer, then, is to determine the "most severe" loading condition which may occur and to apply these forces during the assessment of in-bore structural integrity. By their very nature, the transverse loads, if known, would be dynamic and nonaxisymmetric, unlike the previously defined forces; the stress analysis demands will increase accordingly when these features are finally included. Currently, past experience and a conservative approach must be used to maintain structural integrity of the projectile in the face of local and global bending deformations and vibrations caused by the transverse loadings.

Near or during muzzle exit by the projectile, the base pressure and resultant acceleration are greatly decreased. However, other forces now appear, due to the high velocity, which were negligible at peak pressure. Although the magnitude of these forces is generally such that the time of peak pressure is still the most severe loading environment, these forces may cause problems for ill-conceived designs. Therefore, the muzzle exit condition should generally be investigated for structural integrity also.

The primary example of these additional forces occurs in rifled gun tubes. The high muzzle velocity obtained by saboted projectiles leads to high spin rates, even for despun projectiles. (All modern fin stabilized kinetic energy projectiles fired from rifled guns have their spin rate reduced in some manner so that the fins may survive the encounter with the atmosphere). The resultant high centrifugal body force may cause severe deformations in the segmented sabot petals, especially during muzzle exit.

The high muzzle velocity also generates aerodynamic pressure ahead of the projectile, both in-bore and immediately after muzzle exit. This pressure generally acts on scoops or wings which are intended to cause lift and assist sabot separation after the bore constraint is removed. An accurate prediction of the magnitude of the pressure field acting on the sabot is extremely difficult due to the presence of intersecting shock waves from the subprojectile and individual sabot segments. Rough estimates are based on the stagnation pressures attained through a normal shock at the Mach numbers of interest.

---

[4] *George Soo Hoo and Leon P. Anderson "A Theoretical Model for In-Bore Projectile Balloting," Naval Surface Weapons Center, NSWC TR 79-183, Dahlgren, VA, June 1979.*

Finally, muzzle whip near the time of shot exit may increase the relative importance of transverse loads. This point must remain as speculation until the solution of the coupled projectile/tube motion problem has been attained.

This completes the catalog of loads operating on the projectile to be considered during the design phase. It is the task of the structural engineer to synthesize a configuration of sabot/subprojectile of minimum weight and then to analyze this configuration under the influence of the described forces to ensure that structural integrity is maintained.

Other loads may exist, but they are often the result of problems elsewhere in the system. For example, surging propellant impacting the base of the projectile, large magnitude pressure waves in the gun chamber, or nonaxisymmetric ignition with transverse pressure gradients are potential sources of loading arising from poor charge design. These are problems best eliminated by the propulsion designer rather than the structural engineer.

B. Allowable Loads

For the results of the stress analysis, e.g. the computed stresses and strains, to be useful in assessing structural design, some quantitative measure of what constitutes an allowable loading must be selected from among several possible criteria. The relevant loading response parameter from the stress analysis is then compared to its allowable value; if the parameter is within allowable limits, the configuration is said to possess structural integrity*.

In standard uniaxial tensile testing for material properties, such parameters as yield stress and ultimate strength are fairly repeatable for any given material, loading rate, and metallurgical condition. Under service conditions in a projectile however, the loading is multiaxial. That is, a small cube of material isolated from the structure would have to be loaded over all of its surfaces to be maintained in an identical stress state. For this type of stress field, the comparison of individual normal stress components with the values of uniaxial yield stress or ultimate strength is inappropriate due to the coupling effects with the other stress components. For example, a compressive stress will tend to magnify tensile stresses which act orthogonal to it.

There should of course also be perfect correlation between possession of structural integrity and the subsequent lack of "structural" failures during projectile testing. Poor correlation reflects either unrealistic modeling in the stress analysis, poorly selected allowable loading parameters, or the erroneous identification of the test failure as structurally caused.

What then is the appropriate quantity, calculated from relevant stress analyses of projectiles, to compare with material properties defined by uniaxial tests? Extensive research has been performed to answer this question, which is fundamental to the mathematical theory of plasticity. In that discipline, it is shown that a parameter called effective or equivalent stress combines the effects of orthogonal stress components into a single number which is directly comparable to uniaxial tensile data[5]. Several possible definitions exist for this parameter; in terms of principal stresses.

$$\sigma_{eff} = \sqrt{\frac{1}{2}} \sqrt{(\sigma_1 - \sigma_2)^2 + (\sigma_2 - \sigma_3)^2 + (\sigma_3 - \sigma_1)^2} \quad \text{(Von Mises)}$$

or

$$\sigma_{eff} = \text{Max} \left\{ (\sigma_1 - \sigma_2) , (\sigma_2 - \sigma_3) , (\sigma_3 - \sigma_1) \right\} . \quad \text{(Tresca)} \tag{4}$$

The Von Mises definition is generally preferred, but the Tresca is used occasionally for its analytical simplicity when the maximum difference is known a priori.

Before comparing values of this parameter to any allowable stress from a uniaxial tensile test, it must be verified that the simple tensile test corresponds to roughly the same loading conditions in terms of temperature and loading rate. For the most used metals (plastics are another matter) the ambient temperatures of interest in projectile testing, -50°F to 145°F, (-45°C to 63°C) do not greatly affect the shape of the stress-strain curve. Fracture toughness may decrease if the lower temperature is below the transition temperature; other properties have only minor variation. If we were required to use the metal at an ambient temperature corresponding to the propellant flame temperature, the situation would of course be very different. However, the projectile is exposed to this high temperature for only a few milliseconds. Unless there is rapid gas flow over the solid surfaces, there is no appreciable heating of the projectile during in-bore travel.

Likewise the rate of loading effects at extremely high strain rates (impact loading) may significantly raise the static yield strength of some materials. At the moderate rates associated with in-bore projectile travel, however, the strengthening effect is generally negligible for metals.

---

[5] *Alexander Mendelson, Plasticity: Theory and Application, Macmillan Co., New York, NY, 1968.*

After an appropriate measure of loading intensity has been selected, its limiting value must be set. One possible limit is the value of stress where plastic flow begins, the yield stress. This limit is commonly used for structures subject to repeated service, but is often ignored for projectiles on the ground that they represent a "single use" item and that residual plastic deformation after use is irrelevant. However, each projectile is actually a "double use" item; in addition to launch, it must also function at the target. Large amounts of plastic work during the launch phase could change the material properties of the penetrator from the metallurgically determined optimum for penetration. Whether smaller scale yielding would also be detrimental is unknown, but the conservative course would be to maintain elastic response in the penetrator during launch. The shape of the stress-strain curve will partially determine the suitability of plastic yield as a limit value, since a small plastic work-hardening slope would give a corresponding small margin of safety.

Margin of safety for the stress level is an important concept when the complete loading is as poorly known as indicated previously. To define this alternate stress limit, some fraction of the minimum ultimate strength of the material is specified, e.g. one half. The fraction defines the safety factor used in the design and may be selected arbitrarily by the structural designer based on his subjective perception of the consequences of structural failure and the requirement for weight reduction of the projectile.

The stress limit utilized in the present investigation has been the minimum of the plastic yield stress and the selected fraction of ultimate strength. This multiple limit allows the designer to maintain both an elastic launch and an acceptable safety factor.

A new discipline which holds the promise of developing a separate measure of acceptable load intensity is fracture mechanics[6]. The use of penetrator materials, even of extremely high strength, whose ductility and/or fracture toughness is small, may result in the occasional failure of projectiles. Some difficulty has been encountered during cold (-45°C) testing of projectiles due to the low toughness of some penetrator materials below their fracture transition temperature. Fracture mechanics principles have been well used in the investigation of this type of essentially metallurgical problem. For the determination of design limits, the specification of the material's fracture toughness and the size of detectable flaws theoretically allows for the easy determination of a maximum working normal stress. However, in the present state-of-the-art, such complications as multiaxial stress fields, high stress gradients, large plastic flow, and coupled modes of fracture have not been dealt with in a satisfactory manner, so a design based solely on

[6] *Fracture Mechanics Design Handbook, U.S. Army Missile Command, Technical Report RL-77-5, Redstone Arsenal, AL, December 1976.*

fracture mechanics principles would be premature.

III. SUPPORTED LENGTH OF PENETRATOR

The supported length of the penetrator, i.e. the length of the sabot, is a major factor affecting the structural integrity of long rod kinetic energy projectiles. For the dense materials commonly used in penetrators and the high acceleration fields encountered at launch, the unsupported length of the subprojectile is severely restricted by the allowable stress limits. True push or pull types of sabots are inappropriate for this reason. Instead, a side-gripping sabot with unsupported subprojectile fore and aft of the sabot will minimize the sabot length.

Before the analysis can proceed, an estimate of the mass of the sabot must be made. This mass estimate when combined with the given subprojectile mass is utilized in two preliminary calculations; first in the Lagrange correction to determine the maximum base pressure acting on the projectile, and second, to determine the acceleration of the projectile under the action of this pressure. Any of several methods for making this initial guess at sabot weight may be used; one such formula is developed in the next section. The simplest estimate is the assumption that a third of the total projectile mass is sabot. (The ratio varies from one quarter to one half for most modern kinetic energy projectiles). Thus, for now

$$M = \frac{3}{2} M_{sp} = M_{sp} + M_s , \qquad (5)$$

where

M_{sp} = specified mass of subprojectile, and

M_s = mass of sabot.

Since the acceleration is so dependent on sabot mass, which may be shown in turn to be largely determined by projectile acceleration, it may be correctly anticipated that the following phases of the design are highly iterative.

The calculation, on the basis of allowable stress in the penetrator, of the unsupported length of penetrator which extends fore and aft of the sabot may be performed by reference to the configuration and nomenclature specified in Figure 1. As mentioned, the total length and diameter of the penetrator and weight of nose cone and fins are assumed to be given. Then, assuming that the stress in the rod immediately ahead of the sabot is uniform, balancing forces on a freebody of the fore length of the penetrator yield

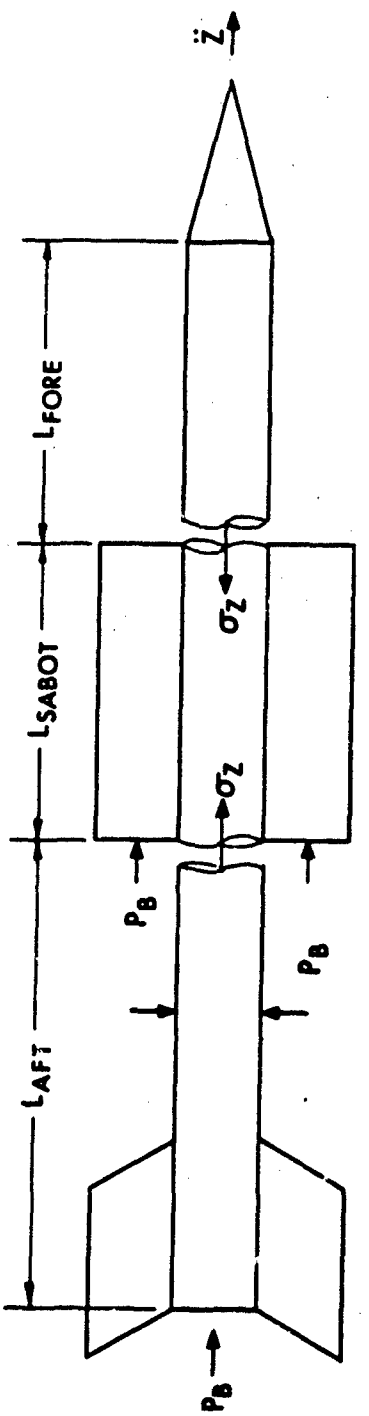

Figure 1. Freebodies Used for Determination of Fore and Aft Unsupported Length of Penetrator

$$\sigma_z A_p + \rho_p A_p L_{fore} \ddot{Z} + M_n \ddot{Z} = 0, \quad (6)$$

where

σ_z = axial stress,

A_p = cross-sectional area of cylindrical penetrator,

ρ_p = density of penetrator material, and

M_n = mass of nose cone.

Since the forward section of the subprojectile is effectively under uniaxial loading, the design limit allowable stress, σ_{allow} must be substituted directly into Eq. (6) (negative for compression) and that expression solved algebraically for L_{fore}

$$L_{fore} = \frac{\sigma_{allow}}{\rho_p \ddot{Z}} - \frac{M_n}{\rho_p A_p}. \quad (7)$$

The situation behind the sabot is slightly different. Here the base pressure also acts on the freebody of the aft length. Summing forces on the aft freebody in the axial direction

$$\sigma_z A_p = \rho_p A_p L_{aft} \ddot{Z} + M_f \ddot{Z} - P_b A_p, \quad (8)$$

where

M_f = mass of fins.

The rear of the penetrator is experiencing a state of multiaxial stress, since the base pressure generates a radial stress, σ_r, here. Using a maximum shear stress (Tresca) condition for effective stress here gives

$$\sigma_{eff} = \sigma_z - \sigma_r = \sigma_z + P_b. \quad (9)$$

Using this result to modify Eq. (8) gives

$$\sigma_{eff} A_p = \rho_p A_p L_{aft} \ddot{Z} + M_f \ddot{Z} \qquad (10)$$

and the insertion of the design stress limit into Eq. (10) for σ_{eff} allows the calculation of the aft unsupported length of the penetrator

$$L_{aft} = \frac{\sigma_{allow}}{\rho_p \ddot{Z}} - \frac{M_f}{\rho_p A_p} . \qquad (11)$$

In the previous calculations the stress over the cross-section of the cylindrical penetrator was assumed to be uniform. This is not the case in actuality; the axial stress approaches some nonuniform radial distribution at the ends of the sabot due to the presence of interface shear stresses within the sabot. This will cause localized stresses above the allowable value specified previously. This local excursion may be ignored, since it is confined to a small volume which may relieve itself to some extent by plastic flow. To maintain the outer surfaces of the penetrator within the design stress limits, the stress values used in Eqs. (7) and (11) may be decreased by approximately 10%.

After the calculation of L_{fore} and L_{aft}, the length of the sabot required to launch the projectile may be found by subtraction from the specified total length of the penetrator, L, which for a cylindrical penetrator is

$$L = \frac{M_p}{\rho_p A_p} , \qquad (12)$$

where

M_p = mass of penetrator.

For slightly tapered, stepped, grooved or otherwise noncylindrical rods, the length L is a ficticious distance corresponding to an equivalent cylinder. Thus,

$$L_{sabot} = L - L_{fore} - L_{aft}$$

$$= \frac{M_p}{\rho_p A_p} - \frac{2\sigma_{allow}}{\rho_p \ddot{Z}} + \frac{M_n + M_f}{\rho_p A_p}$$

$$L_{sabot} = \frac{M_{sp}}{\rho_p A_p} - \frac{2\,\sigma_{allow}}{\rho_p \ddot{z}}, \tag{13}$$

since

$$M_{sp} = M_p + M_n + M_f .$$

Although not generally a factor for high length to diameter penetrators, the sabot length from Eq. (13) must be checked against the length of sabot/penetrator interface required to transfer the total shear load from the sabot. The freebodies used for this check are shown in Figure 2. The total load transfered from the sabot is found by summing forces

$$T = P_b (A_b - A_p) - M_s \ddot{z}, \tag{14}$$

where

T = total shear traction between sabot and rod, and

M_s = mass of sabot ($= \frac{1}{2} M_{sp}$ for initial estimate).

This force must be transferred as a shear stress, τ, over the interface area between the sabot and subprojectile. The actual mechanism for the transfer will be grooves, threads, lugs, or possibly friction surfaces. The maximum shear stress that a material may support, according to the Tresca criterion, is one half of the allowable design stress limit. Due to the discontinuous distribution of sabot and penetrator material and the resultant stress concentrations present in the grooves, the acceptable shear limit across the interface is reduced to one half of this value. Thus the maximum possible value of total shear traction, based on the weaker of sabot or penetrator material, is

$$T_{max} = \pi d_p L'_{sabot} \tau_{max} = \pi d_p L'_{sabot} \left(\frac{1}{4}\ \sigma_{allow}\right), \tag{15}$$

where

d_p = diameter of penetrator.

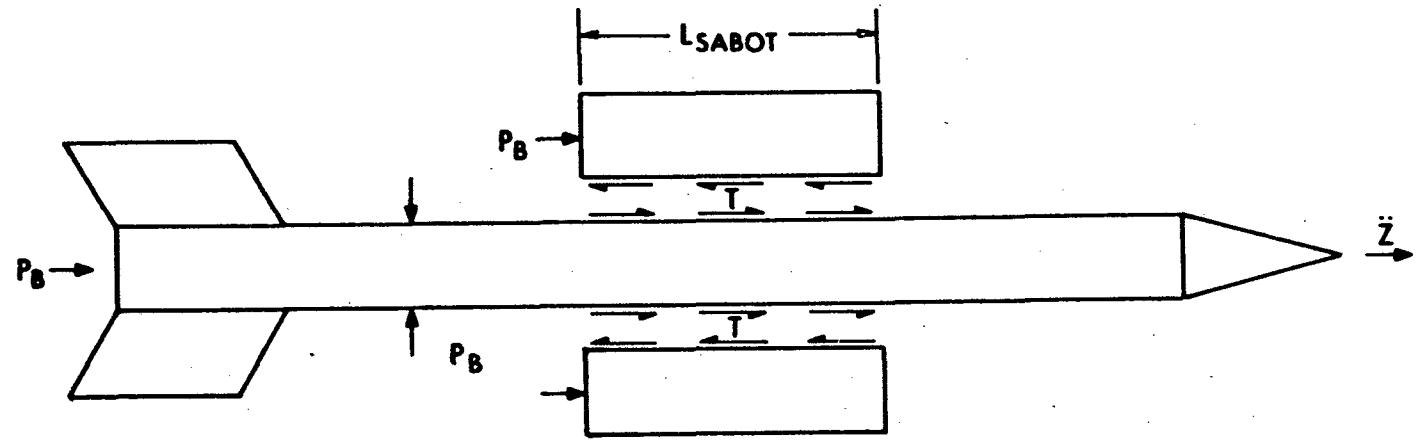

Figure 2. Freebodies Used for Determination of Maximum Shear Traction at Sabot/Penetrator Interface

When this expression for total shear traction is substituted into Eq. (14), an independent determination of sabot length may be obtained

$$L_{sabot} = \frac{P_b d_p}{\sigma_{allow}} \left(\frac{2}{3} \frac{A_b}{A_p} - 1 \right) . \qquad (16)$$

The greater of the two estimates Eq. (13) or Eq. (16) is adopted in subsequent analyses.

In writing the Eq. (14) the implicit assumption that the shear stress was uniform over the entire interface length was used. Stress analyses of typical configurations show that this is an extremely poor approximation. However, it does represent the limiting maximum load carrying ability of the interface, so this value of sabot length corresponds to the absolute minimum acceptable distance.

One final check should be performed for each iteration of sabot length, namely to determine the stability of the forward unsupported length. By referring to Figure 1, it may be recognized that the front section of the rod is effectively a column, fixed at the sabot end and free at the upper end, in an acceleration field. The question of the stability of this column is the same as the determination of the critical height of a tower under gravitational effect. The problem has been solved, e.g. in reference 7, with the result

$$L_{fore}^3 = 7.84 \frac{E_p I_p M}{\rho_p A_p A_b P_b} , \qquad (17)$$

where

E_p = elastic modulus of penetrator, and

I_p = bending moment of inertia of penetrator.

The numerical coefficient is obtained as the root of a Bessel function corresponding to the associated eigenvalue problem.

The critical length of unsupported rod ahead of the sabot will generally be greater than the value of L_{fore} calculated from stress limits.

---

[7] *A.E.H. Love, A Treatise on the Mathematical Theory of Elasticity, Dover, New York, NY, 1944.*

However, many effects may magnify potential stability problems in the unsupported column e.g. transverse loads, eccentricity of the axis of the subprojectile due to manufacturing tolerance or yaw, and spin of the projectile. For these reasons, a large factor of safety should be placed upon the critical buckling length.

Another potential problem may be seen by inspection of Eq. (17). The critical length of unsupported rod is directly dependent on E_p, the modulus of the penetrator material. As long as the rod is maintained in an elastic state during launch, the modulus is the elastic constant. If plastic yield is allowed in the penetrator ahead of the sabot, however, the correct value to use in Eq. (17) is the tangent modulus taken from the plastic portion of the stress-strain curve. For materials with small values of work hardening, the plastic modulus may be several times smaller than the elastic modulus and the critical length for stability may shrink appreciably. In physical terms this would correspond to the creation of a plastic hinge immediately ahead of the sabot.

IV. ESTIMATION OF SABOT MASS FOR KE PROJECTILE

The previous section used a rough estimate of sabot mass ($\frac{1}{2} M_{sp}$) to determine the length of sabot required to launch the projectile. The results of that section may be combined to give a revised estimate of sabot mass, or total projectile mass, for further iterations. Perhaps of equal importance, the ability to rapidly predict sabot mass with a fair degree of accuracy for a wide range of subprojectile and gun system parameters is a requirement for many systems analysis and effectiveness studies.

The basic premise of the following calculation is that the sabot may be approximated by a conical frustrum, which is bore diameter at one end, penetrator diameter at the opposite end, and L_{sabot} in length. The basic configuration is shown in Figure 3. For this shape

$$M_s = a \rho_s L_{sabot} \left[\frac{\pi}{12} (D_b^2 + D_b d_p + d_p^2) - \frac{\pi}{4} d_p^2 \right], \quad (18)$$

where

a = empirical correlation factor,

ρ_s = sabot material density, and

D_b = diameter of bore.

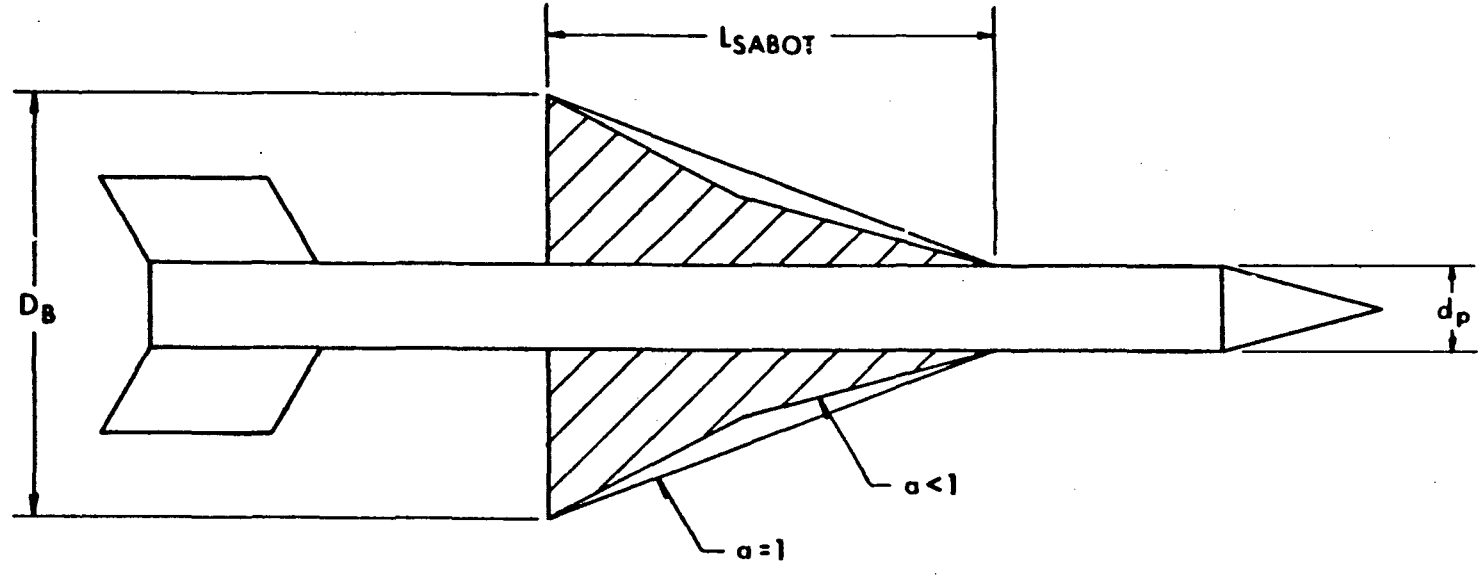

Figure 3. Sabot/Subprojectile Configuration Used for Calculation of Total Projectile Mass

Values of a < 1 may be seen to correspond to weight efficient sabot designs. The sabot length calculated on the basis of allowable stress in the penetrator (generally the most relevant value) may be inserted into Eq. (18). Then defining a subcaliber ratio parameter, Δ, as

$$\Delta = 1 + \frac{d_p}{D_b} - 2\left(\frac{d_p}{D_b}\right)^2 \tag{19}$$

and solving for the total mass of the projectile gives

$$M = \frac{M_{sp}\left[1 + \frac{1}{3}\, a\, \frac{\rho_s}{\rho_p}\, \frac{A_b}{A_p}\, \Delta\right] - \frac{1}{3}\, a\, \frac{\rho_s}{\rho_p}\, \frac{\sigma_{eff}}{P_c}\, C\, \Delta}{1 + \frac{2}{3}\, a\, \frac{\rho_s}{\rho_p}\, \frac{\sigma_{eff}}{P_c}\, \Delta} \,. \tag{20}$$

This expression should be used in place of Eq. (5) for estimates of total projectile mass in further design calculations.

For a generally conservative estimate of projectile mass for use in parametric studies of weapon systems, etc., Eq. (20) may be used with a = 1.0. The remaining factors in the expression are known for a given or proposed weapon system and for specified variations in subprojectile mass, length, and diameter, such as are required in optimizing some measure of projectile performance.

More exact (less conservative) predictions of projectile weight for advanced, weight-efficient sabots may be obtained by including the effects of the materials used in the design. The density of the penetrator and sabot materials is of course an important parameter. However, the efficiency of a sabot material for a particular subprojectile application depends on the ratio of the elastic moduli of the sabot to penetrator. The reason for this is the complex mechanical interaction between these two components during launch. Most of the remainder of this report will be used to review details of this coupling. For now, an effectively empirical function of the elastic moduli ratio may be used to account for the very different relative stiffness of common sabot and penetrator materials. Thus,

$$a_{al} = \frac{1}{1 + .83\, \frac{E_{al}}{E_p}} \,,$$

where

E_{al} = modulus of aluminum, and

E_p = modulus of penetrator material.

The factor was calibrated to aluminum sabots designed according to the method outlined in this report. In dealing with other possible sabot materials, e.g. magnesium or reinforced plastics, their low density should be modified to account for their relatively low modulus. The factor a should also express this "specific stiffness" of any sabot material relative to the calibration material (aluminum).

Since a in the Eq. (20) for projectile mass always appears in the combination $(a\rho_s)$, requiring the product of this factor and specific stiffness to be constant gives

$$(a\rho_s) \quad \frac{E_s}{\rho_s} = \left(a_{al}\rho_{al}\right) \quad \frac{E_{al}}{\rho_{al}}$$

or

$$a = \frac{E_{al}}{E_s} \; a_{al} \; ,$$

where

E_s = modulus of sabot material.

The full expression for a may be obtained as

$$a = \frac{E_{al}/E_s}{1 + .83 \dfrac{E_{al}}{E_p}} \; . \qquad (21)$$

This value of a used in Eq. (20) should account for the effect of variation in sabot or penetrator material on projectile weight, in addition to the variation caused by density changes. Of course if a

specific example of the desired projectile configuration and material combination is available, a may be calibrated to this datum point. Then the Eq. (20) will merely reflect the effects of various subcaliber ratios, penetrator weights, etc. on total projectile mass.

V. DESIGN OF SABOT CONFIGURATION

The sabots used to launch modern kinetic energy penetrators are multisegmented, arranged annularly about the subprojectile to seal the tube while in-bore, and designed to separate into the several segments for discard after muzzle exit. The major types of sabots in current use for long rod subprojectiles are shown in Figure 4.

The most common sabot is the conventional saddle-back type. Its identifying feature is the location of the obturating band in a massive, bore-diameter section at the rearmost position. A forward borerider for transverse support is generally of a bell-shaped section located at the front edge of the sabot. This configuration maximizes the wheelbase of the sabot, i.e. the distance between the boreriding surfaces. For a given clearance between projectile and tube, the longest wheelbase will give the smallest in-bore yaw, if the projectile is treated as a rigid body.

The other type of sabot shown is the double ramp. Identifying features of this sabot are the long conical tapers extending forward and aft from the obturating band. The band is again located in a massive, bore-diameter section, but this section is now located toward the center of the sabot. An additional boreriding surface is also required; this may take the form of a bell located on the front taper or a tapered cylindrical skirt extending forward from the central section as shown.

Several advantages are obtained from the double ramp sabot configuration which assist the designer in meeting the structural integrity requirements. The high pressure propellant gas operates on the rear taper of the multisegment sabot, where it generates high compressive hoop stresses. These stresses clamp the adjacent sabot petals firmly together and to the subprojectile, making the ramp backed configuration essentially self-sealing to the propellant gas. This is in sharp contrast to a saddle-type configuration, which often tends to open the splits between sabot petals due to the action of high base pressures, requiring an additional structural seal to protect against blowby.

A second advantage of the double ramp configuration concerns load transfer under the tapered regions. Most of the force imparted to the sabot by the base pressure must be transferred to the subprojectile. The physical mechanism for this transfer may be grooves, threads, friction surfaces, etc. From a continuum mechanics view the load is transferred by shear stresses across the sabot/subprojectile interface. A saddle configuration with an axially stiff, bore diameter band seat section at the end of the sabot, has a high shear stress concentration

SADDLE-BACK

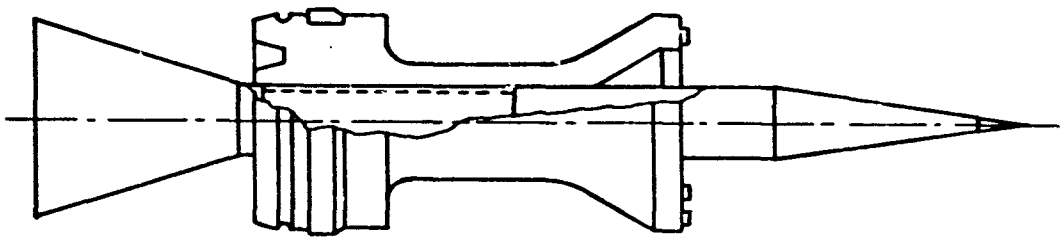

DOUBLE-RAMP

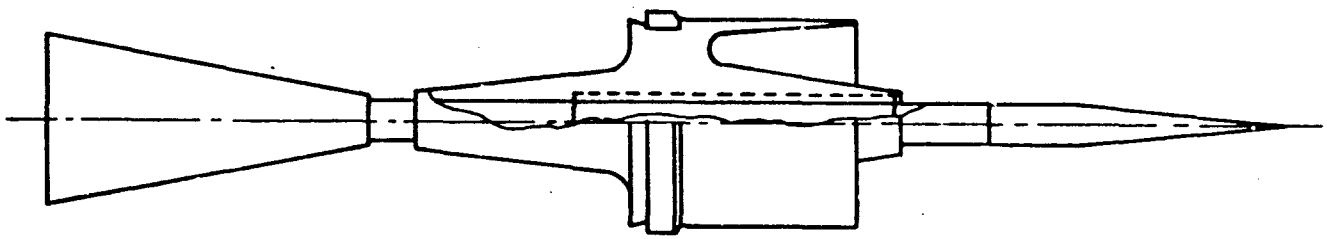

Figure 4. Common Types of Sabots Used to Launch Kinetic Energy Projectiles

at this position. By specifying the exterior taper of the sabot ramp, the axial stiffness may be varied along the sabot so that the stress concentration is eliminated and, in fact, the shear stress variation with axial location is specified to allow maximum load transfer.

A final advantage of the ramp configuration when compared to a saddle appeared in empirical data during the 105 mm Advanced Technology Tank Gun Initiative, in which both types of sabot were developed for essentially identical subprojectiles. The double ramp sabot weighed a full pound less then the comparable saddle sabot, a reduction in parasitic weight of 23%, with corresponding increases in projectile performance.

It is not possible to prove that the double ramp sabot will be a minimum weight design under all circumstances. However, stress analysis of sample configurations presented later in the next section will confirm that the ramp configuration does indeed solve the two indicated structural integrity problems encountered by saddle type sabots. Therefore, the remainder of this chapter on design of the sabot will concentrate on the principles required to determine the exterior profile of a double ramp sabot. Only methods for calculating the tapers at either end of the sabot will be presented.

As discussed previously, the location of the obturating or centering band in relation to the projectile center of gravity, the position, type, and stiffness of the additional borerider supports, the length and configuration of the wheelbase, etc. are factors of immense importance which vitally influence the transverse in-bore motion (balloting) of the projectile. At the present time no satisfactory design methodology exists which considers the analytical dynamics of a deformable projectile constrained within a vibrating and recoiling gun tube for the purpose of minimizing balloting and initial yaw at the muzzle. A similar situation exists for the aerodynamic analysis of sabot discard and interaction with the flight subprojectile. Although work is proceeding in both these areas[4,8,9,10] designers must rely solely on experience and intuition to

---

[8] *David Siegelman and Peter Crimi, "Projectile/Sabot Discard Aerodynamics," Ballistic Research Laboratory Contract Report ARBRL-CR-00410, December 1979.* (AD #A080538)

[9] *Edward M. Schmidt, "Wind Tunnel Measurements of Sabot Discard Aerodynamics," Ballistic Research Laboratory Technical Report ARBRL-TR-02246, July 1980.* (AD #A088900)

[10] *Burdette K. Stearns, Robert H. Whyte, and William Walton, "In-Bore Structural Dynamic Behavior and Resultant Dispersion Characteristics of 105 mm Projectile-Sabot Systems," Armament Systems Dept., General Electric Co., Burlington, VT. 05402.*

configure the centering band and additional boreriding supports. No attempt will be made to discuss this type of information here.

The tapers toward the ends of the sabot are not chosen arbitrarily, rather they are calculated to give a specific variation of axial stiffness. This variation in sabot stiffness, in turn, is specifically selected so that the transfer of shear stress from the sabot to the subprojectile will have a favorable axial variation, optimally a constant value with no stress concentrations. (For a given length of sabot/penetrator interface, the maximum load is transferred when the shear stress is equal to the largest permissible value along the entire interface). The methodology which allows the shear stress transfer to be controlled by specifying the taper profile is based on elementary free body analyses such as are used in strength of materials. The basic procedure was developed for single ramp sabots by Dr. B.P. Burns of BRL during the 60 mm AAAC Technology Program[11]. Freebodies are formed from a typical projectile shown in Figure 5 by planes perpendicular to the projectile axis. The freebodies are thin discs of sabot and penetrator material, so thin that squares and higher powers of Δz may be ignored. In addition, the change of external sabot radius with axial coordinate is assumed small by the same type of criteria on $\frac{dR}{dz}$.

The stresses, base pressure and acceleration loads acting on the freebody are also shown in the figure. Propellant gas pressure acts on those parts of the projectile aft of the obturating band. Thus it affects the rear taper but not the forward one. The base pressure and projectile acceleration are known quantities for a specified projectile mass by the methods presented earlier. The ramps are designed to give uniform shear traction at the most severe loading condition, when the shear which must be transferred is a maximum. The axial stresses are taken to be the average over the appropriate axial section and thus do not vary in the radial direction. The shear stress, τ, is the load being transferred from the sabot to the penetrator. It may be set to any value selected by the designer, and will have no variation in the axial direction. Any variation of shear stress with radius does not figure in the analysis. Quantities appropriate to the sabot are indicated by subscript s and those of the penetrator by subscript p in the following derivations.

The purpose of the present calculation is to determine the proper variation of the external radius of the sabot with axial coordinate, R(z), for a given set of projectile loading parameters, so that the shear stress at the sabot/penetrator interface is constant under the entire ramp segment. If a shear traction other than constant is desired for some reason, it may be approximated by a series of step functions, where τ is constant within each axial section.

---

[11] *Bruce P. Burns, "MC-AAAC In-Bore Projectile Technology," Ballistic Research Laboratory Report ARBRL-R-, forwarded for publication.*

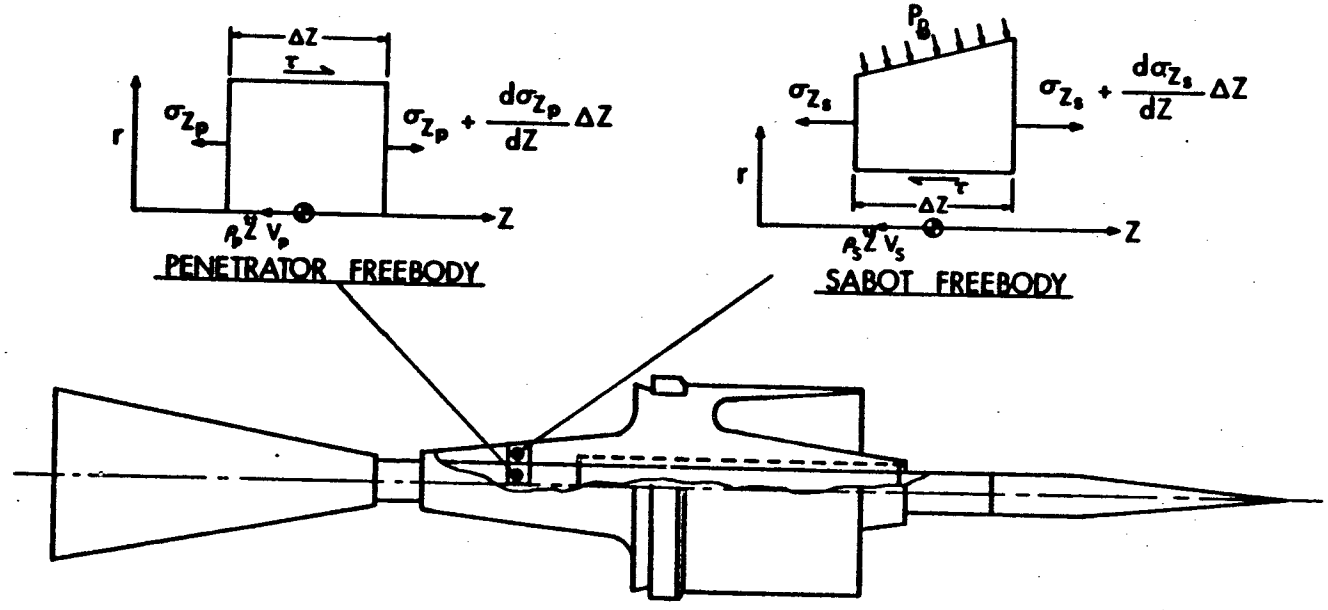

Figure 5. Freebodies Used for Determination of Taper Profile to Give Uniform Shear Stress at Sabot/ Subprojectile Interface

The volume of the conical sabot freebody is

$$V_s = \frac{\pi}{3} \Delta Z \left[R^2 + R\left(R + \frac{dR}{dz} \Delta Z\right) + \left(R + \frac{dR}{dz} \Delta Z\right)^2\right] - \pi R_p^2 \Delta Z$$

$$= \pi \left(R^2 - R_p^2\right) \Delta Z , \tag{22}$$

where terms of $(\Delta Z)^2$ and higher order have been ignored.

Summing the forces acting on the sabot in the axial direction gives

$$\pi \left(R^2 - R_p^2\right)\sigma_{z_s} + 2\pi R_p \Delta Z \tau + \rho_s V_s \ddot{Z} =$$

$$\pi \left[\left(R + \frac{dR}{dz} \Delta Z\right)^2 - R^2\right] P_B + \pi \left[\left(R + \frac{dR}{dz} \Delta Z\right)^2 - R_p^2\right]\left[\sigma_z + \frac{d\sigma_{zs}}{dz} \Delta Z\right].$$

This reduces to (considering the smallness of ΔZ)

$$\left(P_B + \sigma_{z_s}\right) \frac{dR^2}{dz} + \left(\frac{d\sigma_{zs}}{dz} - \rho_s \ddot{Z}\right)\left(R^2 - R_p^2\right) = 2 R_p \tau.$$

Let

$$\phi = R^2 - R_p^2, \text{ and}$$

$$\alpha = \frac{d\sigma_{zs}}{dz} - \rho_s \ddot{Z}.$$

Then the governing differential equation for the determination of R (or ϕ) may be written

$$\left(P_B + \sigma_{z_s}\right) \frac{d\phi}{dz} + \alpha\phi = 2 R_p \tau \tag{23}$$

with initial thickness of sabot specified as initial condition

$$\phi = \phi_o = R_o^2 - R_p^2 \text{ at } Z = 0.$$

To be able to integrate this expression, the variation of σ_{z_s} with Z and the known parameters must be specified.

The summation of the axial forces on the freebody of the penetrator gives

$$\pi R_p^2 \sigma_{z_p} + \rho_p V_p \ddot{Z} = 2\pi R_p \Delta Z \tau + \pi R_p^2 (\sigma_{z_p} + \frac{d\sigma_{zp}}{dz} \Delta Z),$$

which reduces to

$$\frac{d\sigma_{zp}}{dz} = \rho_p \ddot{Z} - \frac{2\tau}{R_p}. \tag{24}$$

This expression is readily integrated to yield

$$\sigma_{zp} = (\rho_p \ddot{Z} - \frac{2\tau}{R_p}) \; Z + \sigma_o. \tag{25}$$

The axial stress in the penetrator is thus a linear function of Z. Its value at the beginning of the sabot, σ_o, was determined when the length of sabot was calculated.

To relate the axial stresses in the sabot and penetrator, the deformations in these unequally stiff components must be compared. Thus, along the interface between the sabot and penetrator the axial displacement must be the same in both components (no slip condition).

$$U_p = U_s \quad , \quad r = R_p.$$

Differentiating along the interface gives

$$\left.\frac{dU_p}{dz}\right|_{r=R_p} = \left.\frac{dU_s}{dz}\right|_{r=R_p} ,$$

which is the same as

$$\epsilon_{z_p} = \epsilon_{z_s} \quad , \quad r = R_p .$$

Rewriting the axial strains in terms of the stresses by using Hooke's Law for elastic materials gives

$$\sigma_{z_s} = \frac{E_s}{E_p} \left[\sigma_{z_p} - \nu_p(\sigma_r + \sigma_\theta)_p\right] + \nu_s (\sigma_r + \sigma_\theta)_s , \tag{26}$$

where

ν = Poisson's ratio.

It remains to determine the quantity $(\sigma_r + \sigma_\theta)$ for the sabot and penetrator in terms of the known pressure and material properties. The exact elasticity solution of a tapered bimaterial ramp under external pressure is beyond the scope of the present analysis. Major simplification is achieved by assuming that this transverse stress field is adequately represented by the solution to the comparable problem in a cylinder (the Lame solution). However even this result is overly complicated, due to the appearance of the external radius in the expression for the transverse stress components $(\sigma_r + \sigma_\theta)$. If this representation were used in the differential Eq. (23), the coefficients would become highly nonlinear functions of R (and ϕ) and the equation could not be integrated in closed form. Since the purpose of the present derivation is to develop a simple design relation for the taper profile, an additional simplication is required.

The appropriate (gross) assumption is to ignore the bimaterial character of the cylinder, for the calculation of the transverse stress components only. This is the only consistent way to remove a dependence on the exterior radius of the configuration from the equation. The error involved is not significantly greater than that due to other assumptions adopted in the analysis, as may be determined by comparison with finite element stress analysis of typical configurations. Then, both σ_r and σ_θ are equal to the external pressure and

$$(\sigma_r + \sigma_\theta)_s = (\sigma_r + \sigma_\theta)_p = - 2P_B . \tag{27}$$

When this expression is inserted into Eq. (26), the revised expression is

$$\sigma_{z_s} = \frac{E_s}{E_p} [\sigma_{z_p} + 2\nu_p P_B] - 2\nu_s P_B. \qquad (26)'$$

The parallel mechanical system being studied has equal average axial strain in the sabot and penetrator. This requires that the relation Eq. (26)′ between material properties, external pressure, and axial stresses be maintained. If the average axial stress in the sabot is changed from this value, for example by the addition of a forward, bell-shaped bore-rider, without sufficient additional stiffness being added to the taper, the system will attempt to maintain this relation by altering the shear transfer between components. Finite element analysis of typical configurations indicate that these conclusions are not artifacts of the methodology, but are indeed approximately true. When the sabot taper and loading conditions are such that Eq. (26)′ is maintained, the shear stress τ at the interface will be of the desired constant value.

Using Eqs. (25) and (26)′ to specify the coefficients of the governing differential equation in terms of the known parameters and z gives

$$(P_B + \sigma_{z_s}) = \frac{E_s}{E_p} [\sigma_o + (\rho_p \ddot{Z} - \frac{2\tau}{R_p}) Z + 2\nu_p P_B] + (1 - 2\nu_s) P_B, \text{ and}$$

$$\alpha = \frac{E_s}{E_p} (\rho_p \ddot{Z} - \frac{2\tau}{R_p}) - \rho_s \ddot{Z}.$$

The Eq. (23) may now be integrated to yield an elementary solution for ϕ. Thus

$$\phi = [\phi_o - \frac{2\tau}{\alpha} R_p] [\frac{\Sigma_o}{\Sigma_o + (\rho_p \ddot{Z} - \frac{2\tau}{R_p}) Z}]^{\beta} + \frac{2\tau}{\alpha} R_p, \qquad (28)$$

where

$$\phi = R(Z)^2 - R_p^2,$$

$$\Sigma_o = \sigma_o + 2\nu_p P_B + \frac{E_p}{E_s} (1 - 2\nu_s) P_B, \text{ and}$$

$$\beta = \frac{E_p}{E_s} \frac{\alpha}{\rho_p \ddot{Z} - \frac{2\tau}{R_p}}.$$

To reiterate the significance of the preced[illegible], a sabot with taper contour given by R(z) computed from Eq. (28) will transfer a constant shear stress τ from sabot to the penetrator over the length of the tapered ramp. This favorable circumstance occurs because the axial stiffness of the sabot is continuously varying due to its increasing thickness. The differential in force at each axial section is dumped onto the penetrator as shear traction. To raise or lower the value of τ, it is merely necessary to use the desired shear traction when computing R by the Eq. (28).

Up to the present the derivation has implicitly considered the rear taper. However, the same analysis applies to the forward taper. Since no propellant gas acts ahead of the obturating band, the base pressure is zero here. In using the formula for ramp profile, the taper begins at the origin of the z axis. Thus the slope of both front and rear tapers is positive. Care must be taken with the sign of other quantities, however, especially the shear τ and acceleration $\ddot{Z}$, depending on the taper under consideration.

The taper profile given by Eq. (28) is nonlinear. Under common conditions the profile is S-shaped and increasing, see Figure 6. The minimum slope of the curve is located slightly away from the end of the taper and the slope increases at a steadily increasing rate after this minimum. In practice it is generally possible to approximate the initial profile by a linear taper corresponding to either the minimum slope or a secant of the curve, while preserving a nearly constant shear transfer (Figure 6). The replacement of the curved taper by a conical segment greatly simplifies dimensioning and machining of the sabot.

Included in Figure 6 is an indication of the direction in which the taper profile is shifted by modification to selected parameters. It is of course important for the minimization of parasitic sabot mass that the taper be as small as possible. The value of Σ_0 is fixed by the base pressure for the system and the axial stress allowed in the rod at the beginning of the sabot, i.e. the length of sabot (See Section III.)

Another factor of major importance in regard to the steepness of the tapers is the ratio of elastic moduli in sabot and penetrator. For an aluminum sabot, this ratio will vary from 0.2 for a tungsten alloy penetrator to a value of 0.5 for depleted uranium. This range of variation has significant influence on the steepness of taper required to give a uniform shear transfer for the different penetrator materials. The difficulty in designing a sabot for use with interchangeable penetrator materials arises from this effect. The problem will be examined in greater detail in the next section.

The influence of sabot material modulus on the steepness of the tapers indicates an area of potential major sabot weight reduction from the utilization of modern materials. Uniaxially stiffened composites, e.g. graphite fiber reinforced plastic or ceramic fiber reinforced aluminum, allow large increases in axial modulus without excessive

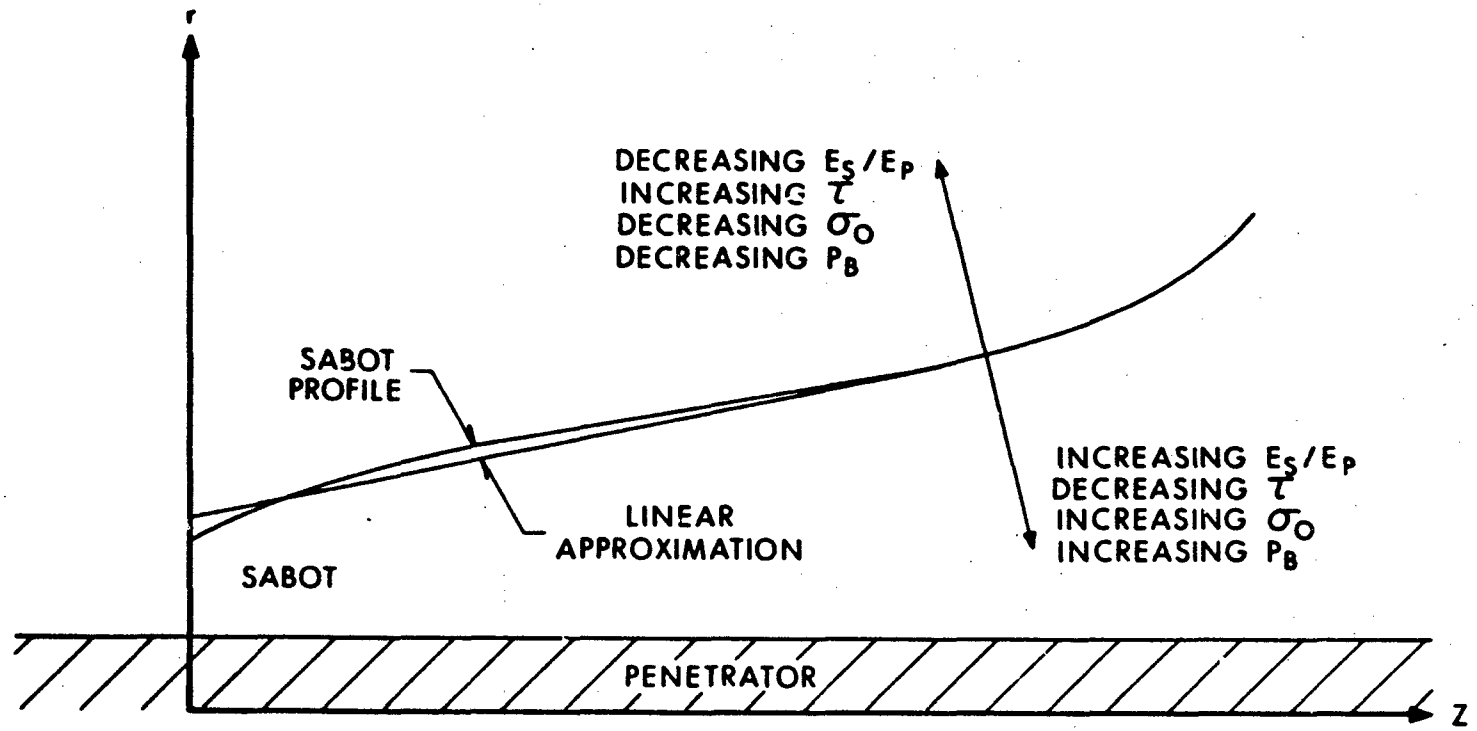

Figure 6. Influence of Major Factors on Taper Profile

weight penalties over the base material. The derivation of the ramp shape performed in this section implicitly assumed an isotropic material, but only the axial modulus was explicitly used. Eq. (28) should thus be applicable for use with these highly anisotropic materials.

The final parameter to be examined is the shear stress, τ, transferred from sabot to subprojectile. Some judgment on the part of the designer enters into the selection of an appropriate value for τ. For example, a uniform traction could be carried over the entire interface between sabot and penetrator. However, the slopes required to give these relatively high shears in the tapered zones would be steep, resulting in an excessively heavy sabot. For this reason a uniform shear over the entire interface is seldom desired. Rather the tapers are calculated to yield some minimum "acceptable" value of shear, constant only under the tapers. The remaining shear load is transferred at the central, band-seat section of the sabot. Thus the zone of higher shear stress is located away from the zone of high axial stress, resulting in a more uniform distribution of effective stress in the penetrator. This minimum "acceptable" shear is determined by several factors, including the ability of the sabot/penetrator interface in the central non-tapered section to carry the increased shear tractions, the stresses and stress concentrations in the rod, and the perceived need to lower sabot weight. The correctness of the designers estimate of minimum shear traction may be determined only after more detailed stress analysis.

An absolute minimum shear traction, and corresponding slope, may be determined as that value which is required to maintain the axial stress in the rod constant and not increasing in absolute magnitude due to the axial acceleration. This traction is minimal because the effective stress in the rod at the beginning of the sabot was equated to the allowable design stress. Hence the stress intensity under the tapers cannot increase without violating the allowable stress condition. This minimum value of shear traction may be obtained from Eq. (25) by requiring that σ_{z_p} be a constant in Z, so that

$$\tau = \tfrac{1}{2} R_p \rho_p \ddot{Z}. \tag{29}$$

For this value of τ the solution of Eq. (28) becomes indeterminate. returning to the governing differential Eq. (23) with this expression for τ yields

$$\phi = \left[\phi_o + \frac{\rho_p}{\rho_s} R_p^2\right] \exp\left[\frac{E_p}{E_s} \frac{\rho_s \ddot{Z}}{\Sigma_o} Z\right] - \frac{\rho_p}{\rho_s} R_p^2, \tag{30}$$

where the quantities are as previously defined.

There may well be valid reasons to design a taper with higher values of shear traction, and hence slope, than is indicated in Eq. (30). For example, the interface under the remaining non-tapered segment of the sabot may not be able to accomodate the increased shear traction caused by the lower values under the ramps. This expression does determine, however, the minimum locus of the profile for the tapered sections.

The analysis leading to Eqs. (28) and (30) could certainly be improved. For example, the transverse stress field due to the base pressure was approximated in a rather cavalier manner. However, it would be inappropriate to develop the strength of materials analysis too far. Its purpose is only to give an initial estimate of a taper profile which permits uniform shear traction to occur at the sabot/penetrator interface. The estimate of the formulae should be checked and improved, if necessary, by iterations of a finite element solution of the complete solid mechanics problem. Only by this procedure may the preceding analysis be justified.

Besides indicating the adequacy of the shear traction variation attempted by the designer, the finite element solution will also give the stress field in the sabot. The structural integrity of the sabot itself is an area which has not been discussed explicitly during the previous approximate analysis. However, estimates of the global stresses in the sabot were developed and so the stress intensity, at least in the ramp sections, may be found. The axial sabot stress is given by Eq. (26)', repeated here

$$\sigma_{z_s} = \frac{E_s}{E_p} \left[\sigma_{z_p} + 2\nu_p P_B\right] - 2\nu_s P_B.$$

For most combinations of sabot and penetrator materials in common use, the ratio $\frac{E_s}{E_p}$ will be such that for reasonable levels of σ_{z_p}, the stress in the sabot will be low enough not to cause severe problems. This condition may of course be altered by use of advanced materials, e.g. fiber-reinforced composites with high modulus, or low strength sabot alloys. In any event, these estimates are only for global stress fields, and local factors such as bending in the root of the forward borerider or the radii leading into the central band seat section must be carefully considered. These features appear only in the more complete finite element analysis.

At this point a digression on the philosophy guiding the design methodology is appropriate. It has been pointed out that the forward unsupported length of subprojectile is determined by the allowable stress in the penetrator. Exceeding the yield stress forward of the sabot is easily recognized as causing potential plastic flow and stability problems. It is sometimes believed, however, that high values of compressive stress in the rod may be tolerated within the sabot. This could be achieved by having the slope of the forward ramp less than the theoretical minimum

value. Plastic buckling and unconstrained flow are prohibited by the sabot. Indeed the reduction in elastic penetrator modulus due to plastic flow (tangent modulus) tends to be self-controlled to some extent, since the shear traction increases under a fixed taper after yield occurs. At first glance, no harm would be caused by this nonconservative approach. If the axial loads were the only ones acting, the risk would be, in fact, small. However, transverse forces of an unknown magnitude are also acting on the projectile. These forces must be balanced by bending moments within the projectile; at the section of highest plastic compressive stress, the ability to generate restoring moments is greatly reduced. Hence, although no part of the present analysis can demonstrate a lack of structural security for this design scheme, it is not recommended as viable. Given sufficient testing, any nonconservative design principle should eventually surface as apparently random structural failures.

VI. EXAMPLES OF SABOT DESIGN

The present section will apply the results obtained in the previous sections to two separate examples of sabot design. The problems investigated will include the selection of sabot type and the difficulty inherent in designing sabot for interchangeable penetrator materials.

The advantages of the double ramp over the more conventional saddle sabot may be illustrated by a finite element analysis of the two configurations. Figure 7 shows a sketch of the somewhat stylized shapes used. The tapers on the double ramp sabot are as calculated by Eq. (28) to give a uniform shear stress. The axial stress, sabot length, base pressure, and materials were identical in the two calculations. Since the masses are significantly different, it would be impossible to include acceleration in this direct comparison, so no acceleration is applied in this example.

A dot is used in Figure 7 to locate each element in the finite element grid of the sabot that has a tensile hoop stress. Since these are both multisegmented sabots which cannot support hoop tension, the seams between the sabot petals in these regions would open to relieve the stress. If the regions are adjacent to surfaces acted on by base pressure, the opening splits would form a path for the hot propellant gas. For the saddle configuration, a path of this type may be followed completely through the sabot, making in-bore blowby of propellant gas a certainty without an additional structural seal. For the ramp sabot, the pressure acting on the rear taper creates highly compressive hoop stress in all adjacent material, illustrating the previously described self-sealing nature of this type of sabot.

Also shown in the figure is a plot of the shear traction at the sabot/rod interface. The shear for the double-ramp configuration is relatively uniform and reflects somewhat the accuracy which is attainable from the approximate design methodology. The shear for the saddle sabot is highly variable, with sharp stress concentrations at the ends and a region of negligible shear transfer in the center.

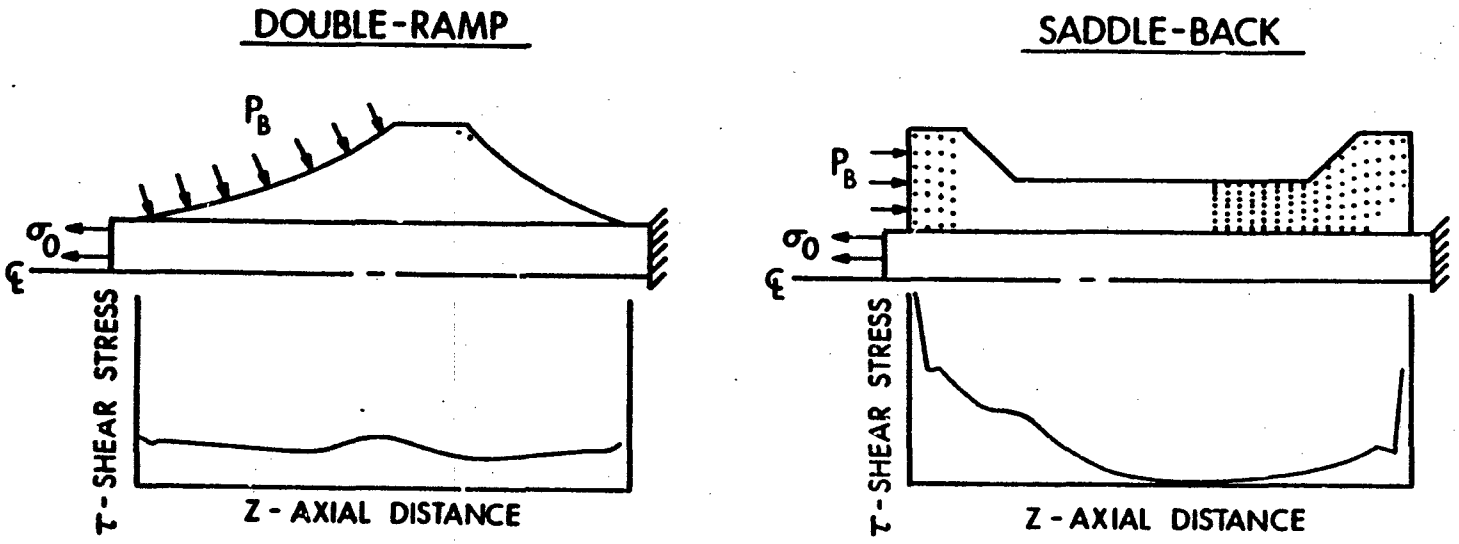

Figure 7. Shear Stress Distribution and Zones of Tensile Hoop Stress in Generic Sabot Types

The high shear concentration in the saddle sabot raises a familiar problem for the structural designer. Grooves at the highly loaded portion of the interface could shear away. The apparent solution is the design of stronger and stronger grooves to carry the existing load, i.e. the solution is commonly based on the consideration of only a single component of the problem. The existence of the high shear traction concentration as a result of the interaction of sabot and penetrator should be recognized as the underlying difficulty. Then the methods of the previous section may be applied to obtain an appropriate solution.

Another solution to the problem of high localized shear tractions, which is sometimes proposed, maintains that no problem exists. The following scenario for groove failure is postulated. As grooves in the high shear zone are being loaded, a maximum traction will be applied which will "yield" these grooves. The "yielded" grooves will continue to carry this load, while any additional traction due to the shear concentration will be spread over adjacent grooves. This process is seen as being repeated until a uniform shear of sorts is applied along the entire interface. It is unknown at present if this concept would work even in principle. Surely it would be highly dependent on the alloy and temper of the sabot material under the best of conditions. In any event, the method seems to place unwarranted confidence in the structural integrity of already "yielded" (i.e. semi-failed) grooves.

The second example springs from a desire to accelerate the design and development phase of projectile production and to minimize logistic problems inherent in having a multitude of projectiles. These considerations led naturally to the concept of a projectile with interchangeable penetrator materials. Unfortunately, this concept is not so natural from a structural design viewpoint.

The materials which are commonly hoped to be interchangeable are tungsten alloy (Wa) and depleted uranium (DU). Nurturing this hope is the fact that the forms of the two metals often used for penetrator application have nearly equal values of ultimate strength and similar densities. However, few other material properties are comparable. The shape of the stress-strain curve, e.g. the location of yield relative to ultimate stress, is very different for the separate materials. The major difference for the present discussion is in the value of elastic modulus; the tungsten modulus is more than double that of uranium. It may be anticipated that the distribution of shear traction is vastly different for penetrators of these materials in the same sabot. Finite element stress analyses of actual configurations will confirm this suspicion.

The configurations chosen to demonstrate this phenomena are a pair of 120 mm kinetic energy projectiles. One sabot was designed specifically for a depleted uranium penetrator, Figure 8; the second was designed for a tungsten rod, Figure 9. Both projectiles were to have the same configuration of subprojectile and identical launch weights to retain

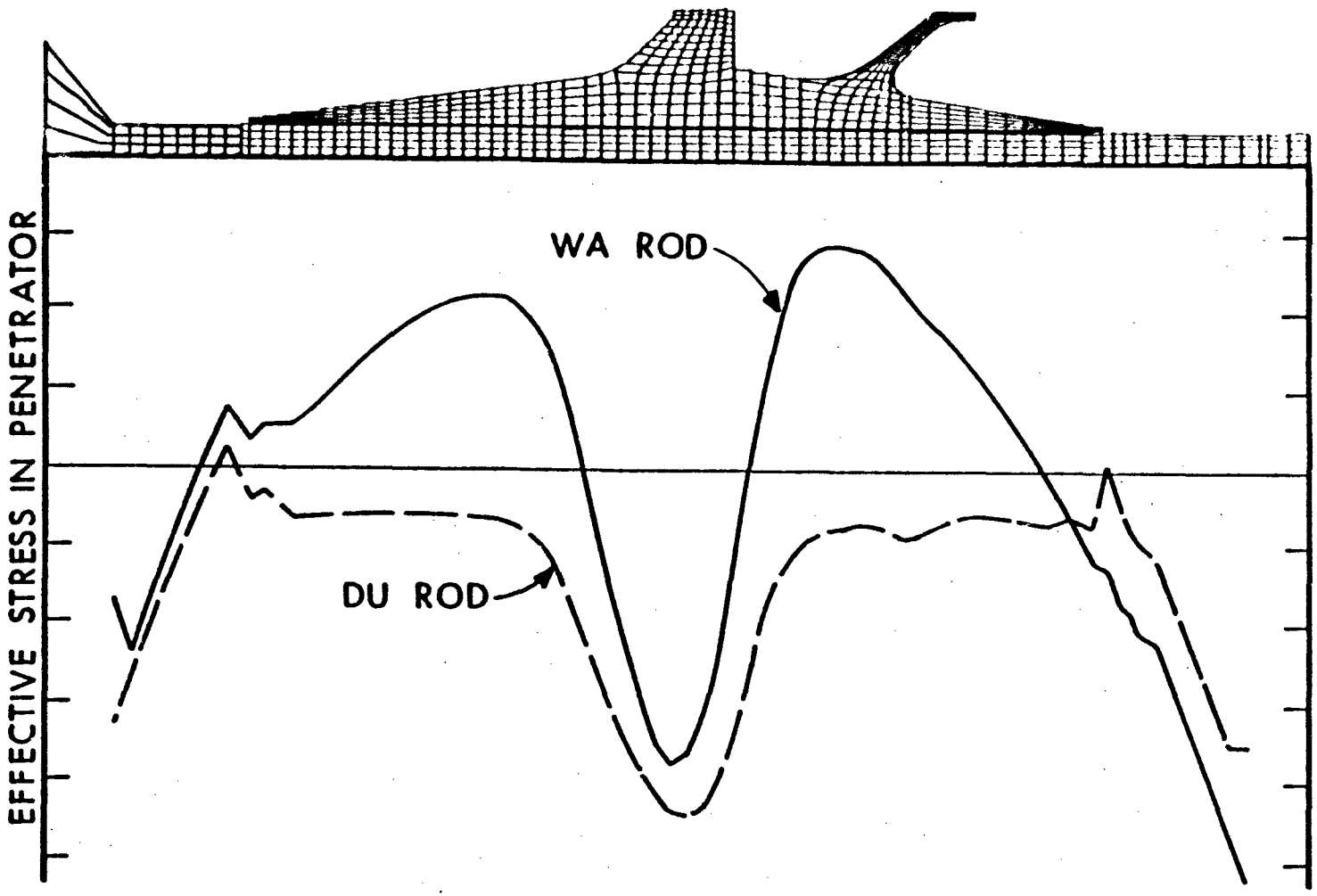

Figure 8. Effective Stress in Penetrators of Tungsten and Depleted Uranium Material During Launch in Sabot Designed for Depleted Uranium Rod

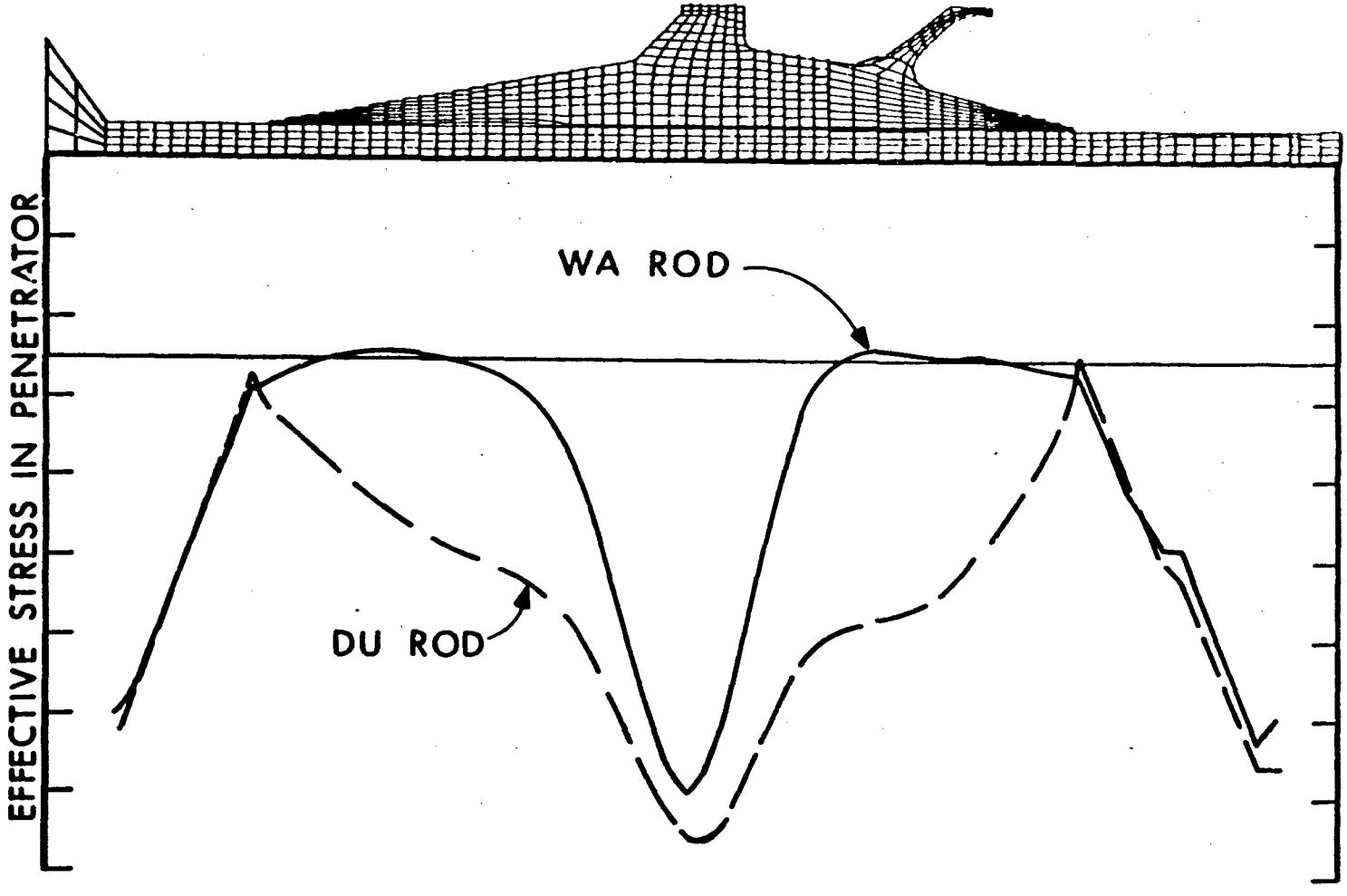

Figure 9. Effective Stress in Penetrators of Tungsten and Depleted Uranium Material During Launch in Sabot Designed for Tungsten Rod

ballistic similarity. Note that the sabot tapers determined for the tungsten subprojectile are steeper and that the sabot length is slightly less than for the depleted uranium design. The steeper slopes yield a sabot which is approximately 10% heavier (the total projectile weight remains the same for the two designs because of the differences in density of the penetrator materials).

The plots in the figures show the variation of effective stress in the penetrator with axial location, while the line represents the design allowable stress selected for each projectile. Figure 8 demonstrates that the DU rod, in a sabot designed for this material, is not stressed beyond its limits. However, for the Wa rod in this sabot, the stress intensity continues to rise within the sabot (due to the insufficient shear transfer from too shallow tapers), considerably above the allowable level.

The situation is different in the sabot designed for a tungsten penetrator (Figure 9). Here the allowable stress limit was set somewhat higher in the penetrator material in an attempt to reduce the excessive sabot weight. Penetrators of both materials satisfy the relaxed stress condition in this sabot and thus demonstrate structural integrity. However, the DU penetrator in this sabot is certainly not a minimum weight configuration. Despite the less conservative structural design, a 10% penalty in sabot weight is added above the configuration of Figure 8.

VII. MECHANISMS OF LOAD TRANSFER AT SABOT/PENETRATOR INTERFACE

The most common method of transferring the shear traction across the sabot/subprojectile interface is by means of annular grooves or threads. This mechanism is not without its drawbacks, however. If the grooves are subcaliber, i.e. cut into the subprojectile, they may seriously lower the terminal performance of the rod by reducing its effective area and serving as stress wave concentrators. If the grooves are supercaliber, i.e. standing above the subprojectile, they adversely effect the aerodynamic performance by increasing the presented frontal area and serving as viscous drag generators. In either case, a high localized stress concentration exists at the root of the groove or thread during in-bore loading, so that this site can serve as a point of fracture initiation for an already highly loaded penetrator. In any event, grooves presently are the only feasible method of transferring high shear tractions over the entire interface during in-bore travel without retarding sabot discard after muzzle exit.

The thread profile which has been found superior over the years for transmitting power in a single axial direction is the buttress. Hence, a slightly modified version of this profile was adapted for use as projectile grooves. The general shape of this buttress groove is shown in Figure 10 for a supercaliber configuration linking dissimilar materials. The computation of dimensions required to specify this configuration will be described.

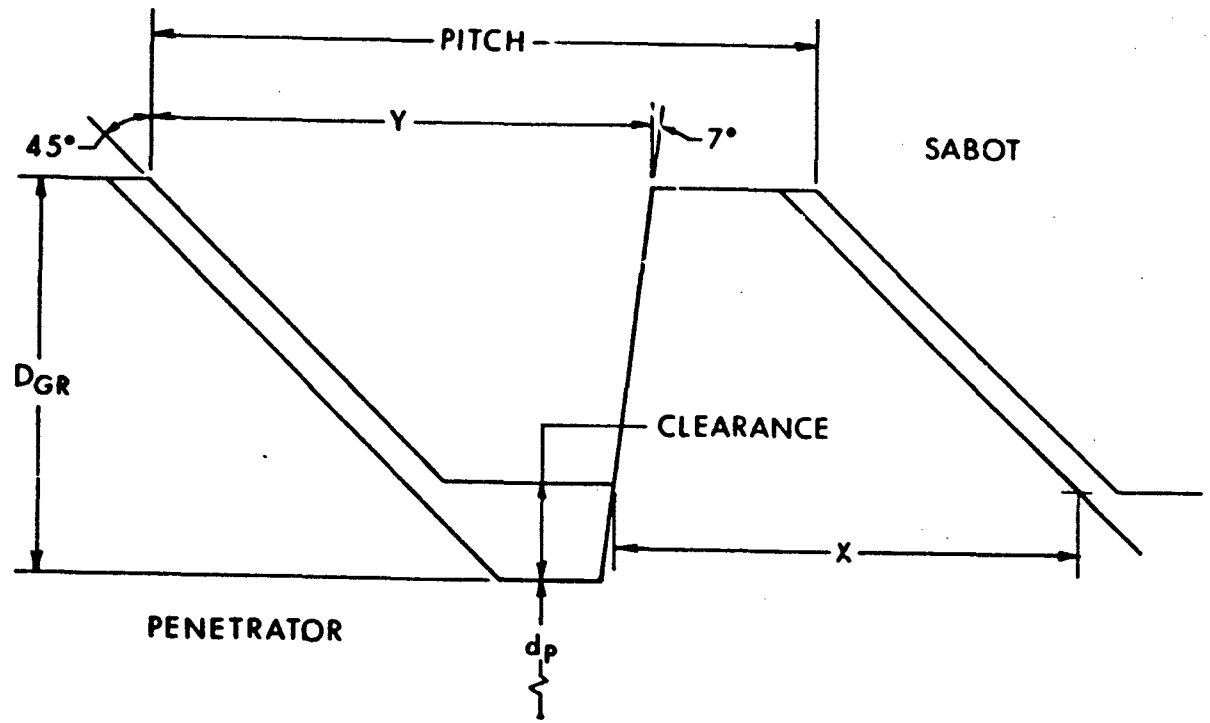

Figure 10. Configuration of Grooves at the Sabot/Subprojectile Interface

Before any grooves are dimensioned, the maximum shear stress at the interface must be determined from a finite element analysis. If a single tooth profile is to be used over the entire interface, this shear traction must be used. If regions of significantly lower shear may be identified along the interface, some advantages, e.g. lower groove height over part of the flight projectile, may be obtained by designing separate grooves in each region.

The maximum shear in any region is converted to force per unit length at the appropriate radius. The design of grooves which may carry this load is then approached by the bearing stress method. A maximum allowable bearing stress in the weaker of the sabot or penetrator material is determined, either by experimental measurements from a typical groove configuration or application of an appropriate factor of safety to published bearing stress data. Dividing the force per unit length to be transferred at the interface by the allowable bearing stress gives groove area per unit length (Strictly speaking, this is axially projected groove area. The 7° slope of the driving face is generally ignored for this part of the calculation)

The groove area per unit length must now be partitioned between grooves per unit length and groove height. This partition is somewhat arbitrary; from a purely theoretical point of view, the groove height should be minimized. The restraint on designs tending in this direction comes from manufacturing capabilities. An overly fine thread is easily damaged during assembly. Of more importance is the effect of manufacturing tolerance. For example, a groove specified to be .025" (1 mm) high with .005" (.2 mm) tolerances on the groove extreme diameters in sabot and penetrator could lose up to 40% of its nominal bearing area by manufacturing variation. The percentage loss for higher grooves is of course less, allowing a less "sloppy" design. In any case, the calculation of bearing area should always be performed with those combinations of tolerances which give minimum permitted contact area between sabot and penetrator tooth. Another manufacturing difficulty which argues against a too vigorous minimization of groove height is the possibility of sabot warpage over the long interface, causing the grooves to partially lift at the ends of the sabot.

A drawback of the bearing stress method of groove design is the illusion that the load transferred across the interface may be increased without limit by increase of the bearing area. The factors limiting the load transfer are the shear strengths of the sabot and penetrator material. Due to the discontinuous distribution of material and the stress concentration in the root of the grooves, the allowable shear stress is considerably less then the tabulated maximum shear stress for the appropriate material without grooves.

Since the allowable shear strength of the weaker material would determine the failure load for equal grooves in dissimilar materials, the design of identical teeth in both materials is inappropriate. Rather

the width of the tooth in the different materials should be proportioned so that the strength of each tooth, from a shear stress criteria, is the same. Thus the ratio of areas represented by the sections at x and y of Figure 10 is set equal to the inverse of the ratio of shear strength of the respective materials. Thus, ignoring the difference in diameter,

$$(\sigma_{allow})_p \; x = (\sigma_{allow})_s \; y. \tag{31}$$

For this calculation, tabulated values of maximum shear should be used, since the stress concentration effects are present in both materials and, hence, do not change the result. If the strengths of the materials are greatly different, some minimum width of tooth must generally be selected for the groove in the stronger material.

The problem with grooves as described above is the high stress concentration generated at the root of the tooth under a combination of high axial and shear stresses. These sites may serve as nucleation points for fracture, especially in materials with relatively small values of fracture toughness. Serious effort must be made to reduce the stress concentrations in these sensitive materials. Filet radii at the root of the tooth should be increased to the maximum size consistent with good fit between components. Preliminary finite element analysis of loading on individual grooves indicates that radial stress applied to the root of the groove tends to amplify the stress concentration, while the same loading applied to the crest of the groove tends to reduce the concentration. For this reason, a groove is normally dimensioned so that the crest of the penetrator groove is in contact with the sabot at one extreme of the tolerance band. At the root of the penetrator groove, however, a sufficient clearance is maintained between the toleranced components so that contact cannot occur.

In addition, a continuing program is being supported within the Army for the development of improved groove profiles[12]. The difficulty commonly encountered in the design of grooves for lowered stress concentration is that the ability of the tooth to transmit axial force is also reduced. Significant advances are possible in this area, however.

One method of avoiding the unfortunate consequences of combined high tensile and shear stresses with the stress concentration due to grooves is available in a ramp-backed sabot. Here the base pressure acting over the rear taper creates high compressive stresses between the sabot and penetrator. With realistic coefficients of friction

[12] *G. Peter O'Hara, "Stress Concentrations in Screw Threads," Large Caliber Weapon Systems Laboratory (Benet), LCLB-TR-80010, April 1980.*

between the dissimilar materials, a smooth interface surface would allow shear tractions to be transferred by a friction drive without the occurrence of localized stress concentrations. The ratio of interface shear to normal stress obtained from a finite element analysis is required to be below some conservatively estimated friction coefficient. At any point along the interface where this ratio exceeds the allowable coefficient of friction, the friction drive is ended and grooves begun. (the concept of a constant coefficient of friction for normal stresses approaching the yield stress of the sabot material can be questioned[13].)

This technique obviously avoids the difficulties of grooves over at least part of the interface. However, there are additional problems which may occur. Many contaminants, e.g. machine oil or graphite from propellant grains, might infiltrate the friction drive during the manufacturing or storage of the projectile, and reduce the shear transferring ability of the interface . Also, contact between the surfaces must be maintained, requiring close tolerances on the friction drive surfaces during manufacture and conceivably implying problems from vibrations and stress waves in components with mismatched dynamic impedences.

VIII. FINITE ELEMENT STRESS ANALYSIS OF PROJECTILE

The strength of materials methods of analysis employed in the previous sections are necessary to allow closed form solutions to complicated boundary value problems. Thus, estimates of the effect of varying any of the parameters included in the analysis may be seen by inspection of these solutions, a vital requirement for the design engineer. Up until recent years, these approximate methods of analysis were commonly used to perform stress analyses of the initial design configuration to determine the structural integrity, for the compelling reason that no other practical method was available. This is no longer the case. Recent developments in computer science and the finite element method have created a situation where a relatively accurate solution to an exactly formulated elasticity (or plasticity) problem may be obtained rapidly and inexpensively. Any designer seriously concerned about structural integrity must take advantage of this ability.

The disadvantage of the finite element method is the same as its advantage, i.e. it solves a boundary value problem in solid mechanics. The computed stresses are presented in the same format whether the incorrect formulation or the correct one is solved. Prof. E.L. Wilson of the University of California reportedly called his highly regarded Structural Analysis Program by the acronym SAP to remind the user that no intelligence may be expected from the code itself. A thorough

---

[13] *James O. Pilcher II, and Emma M. Wineholt, "Analysis of the Friction behavior at High Sliding Velocities and Pressures for Gilding Metal, Annealed Iron, Copper, and Projectile Steel," Ballistic Research Laboratory Report 1955, January 1977.* (AD #A035674)

engineering understanding of elementary freebody methods of analysis and of the concept of total state of stress are much more relevant for the application of finite element techniques than is the theoretical mastery of advanced isoparametric elements or convergence in Hilbert space. Thus the physical intuition of the analyst in reducing actual loadings to mathematical boundary conditions, determining the boundary for a particular analysis, and modeling materials and interfaces is the most significant factor in the quality of the finite element analysis, certainly when using any of the commonly available codes.

The requirements of a finite element code able to perform the types of analyses indicated in the preceding sections are not great. Basically the code need only have a 2D axisymmetric, quasistatic, elastic capability to model the major forces acting on a projectile during travel in the bore of a gun. To make the code more accessible for the frequency of use that is desirable, some form of automatic grid generation and preprocessing is very useful to reduce the immense amount of input data required.

If the projectile has been designed by the procedures outlined in this report, both the sabot and penetrator will be at or below stress levels corresponding to plastic yield, so an elastic analysis is completely warranted. At some surface features on the projectiles, it may happen that the localized effective stress will exceed yield by a small amount. For this case, some minimum plasticity model, e.g. bilinear elastic materials, is desirable so that the relaxation of the stress concentration by plastic deformation may be monitored and the occurrence of large plastic flow strictly avoided.

For the calculation of stresses and deformations due to in-bore loading of projectiles, a dynamic analysis is unnecessary. The time duration of the rising portion of the pressure curve due to propellant gases is large compared to the length and speed of sound in the projectile. Hence, stress waves have a minimal effect on the peak stresses achieved under the normal interior ballistic cycle. (If steep pressure waves in the gun chamber or surging granular propellant are present in the system, dynamic impact effects may become of predominant importance. In general, these are problems best avoided rather then designed to survive).

While inertial effects do not need to be modeled by a dynamic analysis, one of the major loadings on a projectile is the body force due to the essentially rigid body acceleration down the axis of the gun tube. No realistic analysis can be obtained without the inclusion of these distributed inertial loads within the projectile. For the same reason, the analysis of spinning projectiles requires a code with an ability to model centrifugal body forces. The standard prccedure for loading a projectile is to fix a nodal point in a boundary element whose stress state is apparent from physical reasoning, then to apply the pressure and inertial forces. If the gage element is being unduly stretched or compressed, the acceleration is changed until the projectile is approximately balanced under the applied loadings.

The basic configuration of the projectile and the applied loadings are both generally axisymmetric, so the two dimensional formulation is adequate for most investigations. However, nonsymmetric effects may occur due to the segmented nature of the sabot. The individual petals behave in an axisymmetric manner only under hoop compression; under circumferential tensile stress, the splits between petals would open, forming stress free surfaces and circumferentially varying stress fields. Some estimate of the global effect of this local petal separation may be obtained by reducing the hoop stiffness in those elements with tension in this component (if the finite element code allows arbitrarily anisotropic material properties). This approximation does not in any way model the local stress field or intensity, of course.

The stress analysis, indeed the entire design process, is generally applied at peak pressure and acceleration during the in-bore travel. Additionally, for projectiles in a rifled tube, an analysis is required at the point of maximum spin, immediately before muzzle exit. Rotation is normally so slow at peak pressure as to be ignorable there, but, at peak velocity the centrifugal force may be a significant factor.

Additional finite element capabilities may be useful if they are readily available. Thus a full 3D code would allow the actual symmetries of segmented sabots to be modeled, rather than the approximate axisymmetric representation. Also transverse loads, whether due to balloting of the projectile, pressure gradients on the fins, or whatever may be applied to the total analysis of structural integrity. Of course, at present, the nature and magnitude of these transverse forces are unknown, so the ability to model them is of somewhat academic interest.

In the same vein, a more rigorous plasticity model would be advantageous not only for those cases where plastic flow of materials does occur, but also for the modelling of closing gaps, sliding along friction surfaces[14] or large deformations of groove zones.

Finite element modelling of structural features such as grooves have several inherent difficulties. For example the method assumes a continuum. Far from being uniform, the groove zone is an interlocking sequence of alternate material parts and air gaps. The displacement pattern is extremely complicated, completely dissimilar from the smooth deformation shape functions assumed for finite element analysis. Whether threads or grooves can in fact be represented accurately in this manner is an unsettled question of great importance.

---

[14] *Bruce P. Burns and Kathleen L. Zimmerman, "Analysis of the XM736, 8-Inch, VX-2, Projectile Base Configuration," Ballistic Research Laboratory Technical Report ARBRL-TR-02207, January 1980.* (AD #B044270L)

IX. RECOMMENDATIONS FOR CONTINUING RESEARCH

In the preceding sections, the structural design and analysis of the double-ramp type of sabot for use with long-rod kinetic energy projectiles have been detailed. Significant increases in the performance of these projectiles may be obtained from the more weight efficient design, without sacrifice of structural integrity. This advance comes from the development of an integrated design philosophy, which treats the projectile as an organic whole whose components are intimately coupled. The principles outlined in the present report have been demonstrated by the successful launching of a multitude of kinetic energy projectiles, ranging in caliber from 25 mm to 120 mm.

Only the basically axisymmetric shape has been recommended. Some advantages in sabot performance have been claimed by proponents of gussets or longitudinal stiffeners to increase the bending stiffness of the sabot petals and of aerodynamic wings to aid in sabot separation after muzzle exit. These nonsymmetric features add significant difficulties to structural design and analysis and to the manufacturing process as currently practiced. Since the potential performance advantages from this increased complexity cannot be quantified, or even demonstrated in most cases with present technology, no attempt was made to describe these details.

The design of obturating bands and band seats is an area in which almost no analytical methodology exists. Among the difficulties encountered is the determination of the configuration of band to give total obturation in worn or gouged gun tubes, the uniform despinning of projectiles fired in rifled tubes, and estimates of the engraving and bore friction forces to allow adequate structural integrity of the band. Realistic modeling of these problems would have to include the large local plastic deformation occurring at high rates in temperature dependent polymeric materials. Time spent on this field would be well spent, however, if a more rational design process for obturating/locating bands were developed.

Another area with rich potential for structural research centers on the design of the shear transferring mechanisms. High local stress concentrations are known to exist in the root of the standard buttress groove. Efforts to reduce this level of stress concentration, while simultaneously maintaining load transfer per unit length of sabot/subprojectile interface, should be made with both analytical and experimental means. An essentially different problem, but also focused on the grooves, is the generation of a continuum model of a thin groove layer which allows the accurate prediction of the global behavior of a body with threaded or friction interfaces.

The testing of certain configurations of kinetic energy projectiles seems to indicate that transverse vibrations may have an effect on the in-bore behavior, especially when a friction drive is relied upon. No

analytical investigation has been performed on this subject, due primarily to the difficulty encountered in modeling the bending of the sabot/penetrator system. Since the system response changes depending on whether tensile or compressive stresses exist across any interface, the bending stiffness of the projectile varies discontinuously throughout a vibration cycle. In addition, the frequency, content and amplitude of the forcing functions, whether due to turbulent propellant gas acting on the fins or balloting impacts with a dynamic gun barrel, are completely unknown.

Certainly the most pressing unsolved problem facing the projectile designer at the present time does not involve structural integrity directly. Rather it is the development of a methodology which allows the rational design of in-bore configurations so that balloting and sabot separation have a minimal effect on the flight of the subprojectile. Two problems exist in this area, closely related but separate. One is the solution of the full, coupled, nonlinear, six degree-of-freedom dynamic equations for the motion of an elastic projectile constrained within a vibrating and recoiling gun tube. This quantitative formulation will surely require elaborate numerical solution when the modeling is finally in hand. The fruit of the labor will be the capability of predicting the accuracy potential of a specified configuration of projectile.

The other, related problem is the development of a design methodology which would allow the synthesis of a projectile configuration which optimizes some measure of subprojectile accuracy. Obviously, to be tractable, the second solution would have to be qualitative and/or highly approximate. For example, a procedure which required the in-bore motion of the unconstrained projectile to be stable might minimize yaw and yaw rate at the muzzle exit. This formulation could then perhaps be inverted to obtain bounds on the physical parameters, such as moments of inertia and location of center of gravity, such that the motion is indeed stable. Whatever the precise methods adopted for solution, these two related problems are surely the most important facing the projectile designer today.

ACKNOWLEDGMENT

The recent design programs for the 105 mm Advanced Technology Tank Gun Initiative and the 120 mm XM829 antiarmor projectiles serve as the foundation of the present report. This work was performed by a team consisting of Richard D. Kirkendall, Louise D. Kokinakis, and the author all of the Interior Ballistic Division of BRL. Additionally, a previous effort on the saboting of kinetic energy projectiles was performed by Dr. Bruce P. Burns of IBD as part of the 60 mm AAAC Program.

REFERENCES

1. Sabot Technology Engineering, Engineering Design Handbook, AMC Phamphlet 706-445, Department of Army, Washington, DC, July 1972.

2. Interior Ballistics of Guns, Engineering Design Handbook, AMC Phamphlet 706-150, Department of Army, Washington, DC, February 1965.

3. John M. Hurban and Stephen G. Sawyer, "Analysis of Effective Band Pressure in the 152 mm Gun Tube Using Finite Elements and Shell Pushing Data," Proceedings of U.S. Army Science Conf., West Point, NY, June 1972.

4. George Soo Hoo and Leon P. Anderson "A Theoretical Model for In-Bore Projectile Balloting," Naval Surface Weapons Center, NSWC TR 79-186, Dahlgren, VA, June 1979.

5. Alexander Mendelson, Plasticity: Theory and Application, Macmillan Co., New York, NY, 1968.

6. Fracture Mechanics Design Handbook, U.S. Army Missile Command, Technical Report RL-77-5, Redstone Arsenal, AL, December 1976.

7. A.E.H. Love, A Treatise on the Mathematical Theory of Elasticity, Dover, New York, NY, 1944.

8. David Siegelman and Peter Crimi, "Projectile/Sabot Discard Aerodynamics," Ballistic Research Laboratory Contract Report ARBRL-CR-00410, December 1979. (AD #A080538)

9. Edward M. Schmidt, "Wind Tunnel Measurements of Sabot Discard Aerodynamics," Ballistic Research Laboratory Technical Report ARBRL-TR-02246, July 1980. (AD #A088900)

10. Burdette K. Stearns, Robert H. Whyte, and William Walton, "In-Bore Structural Dynamic Behavior and Resultant Dispersion Characteristics of 105 mm Projectile-Sabot Systems," Armament Systems Dept., General Electric Co., Burlington, VT. 05402.

11. Bruce P. Burns, "MC-AAAC In-Bore Projectile Technology," Ballistic Research Laboratory ARBRL-R-, forwarded for publication.

12. G. Peter O'Hara, "Stress Concentrations in Screw Threads," Large Caliber Weapon Systems Laboratory (Benet), LCLB-TR-80010, April 1980

13. James O. Pilcher II, and Emma M. Wineholt, "Analysis of the Friction Behavior at High Sliding Velocities and Pressures for Gilding Metal, Annealed Iron, Copper, and Projectile Steel," Ballistic Research Laboratory Report 1955, January 1977. (AD #A035674)

REFERENCES (continued)

14. Bruce P. Burns and Kathleen L. Zimmerman, "Analysis of the XM736, 8-Inch, VX-2, Projectile Base Configuration," Ballistic Research Laboratory Technical Report ARBRL-TR-02207, January 1980. (AD #B044270L)

DISTRIBUTION LIST

No. of Copies	Organization
12	Commander Defense Technical Info Center ATTN: DDC-DDA Cameron Station Alexandria, VA 22314
2	Director Defense Advanced Research Projects Agency 1400 Wilson Boulevard Arlington, VA 22209
1	Director Defense Nuclear Agency Washington, DC 20305
1	Commander US Army BMD Advanced Technology Center ATTN: BMDATC-M P. O. Box 1500 Huntsville, AL 35807
1	Commander US Army Materiel Development and Readiness Command ATTN: DRCDMD-ST 5001 Eisenhower Avenue Alexandria, VA 22333
2	Commander US Army Armament Research and Development Command ATTN: DRDAR-TSS Dover, NJ 07801
5	Commander US Army ARRADCOM ATTN: DRDAR-LCU, E. Barrieres R. Davitt DRDAR-LCU-M, D. Robertson J. Sikra M. Weinstock Dover, NJ 07801
5	Commander US Army ARRADCOM ATTN: DRDAR-LCA, C. Larson B. Knutelski DRDAR-LCR-R, E.H.Moore,III DRDAR-LCA, H. Fair DRDAR-LCS, J. Gregorits Dover, NJ 07801
7	Commander US Army ARRADCOM ATTN: DRDAR-LCW DRDAR-LCE DRDAR-LCM DRDAR-LCN DRDAR-LCS DRDAR-LCU DRDAR-LC Dover, NJ 07801
8	Commander US Army ARRADCOM ATTN: DRDAR-LCM, E. Bloore J. Mulherin DRDAR-SCS, B. Brodman Dr. T. Hung S. Jacobson DRDAR-SCA, W. Gadomski E. Malatesta DRDAR-SCS, D. Brandt Dover, NJ 07801
6	Commander US Army ARRADCOM ATTN: DRDAR-SC DRDAR-SA DRDAR-SCM DRDAR-SDS DRDAR-SCA DRDAR-SCF Dover, NJ 07801
1	Commander US Army ARRADCOM ATTN: DRDAR-SE Dover, NJ 07801

DISTRIBUTION LIST

No. of Copies	Organization
2	Commander US Army ARRADCOM Product Assurance Directorate ATTN: DRDAR-QA Dover, NJ 07801
2	Commander US Army ARRADCOM ATTN: Development for Project Ofc for Selected Ammunition DRDAR-DP Dover, NJ 07801
3	Commander US Army ARRADCOM ATTN: DRDAR-TD DRDAR-TDA DRDAR-TDS Dover, NJ 07801
1	Commander US Army ARRADCOM ATTN: Army Fuze Mgt Proj Ofc DRDAR-FU Dover, NJ 07801
1	Commander US Army Armament Materiel Readiness Command ATTN: DRSAR-LEP-L, Tech Lib Rock Island, IL 61299
5	Director US Army ARRADCOM Benet Weapons Laboratory ATTN: DRDAR-LCB (2 cys) DRDAR-LCB-TL DRDAR-LCB, Dr.T.Davidson DRDAR-LCB, Dr. J. Zweig Watervliet, NY 12189
1	Commander US Army Aviation Research and Development Command ATTN: DRDAV-E 4300 Goodfellow Boulevard St. Louis, MO 63120

No. of Copies	Organization
1	Director US Army Air Mobility Research and Development Laboratory Ames Research Center Moffett Field, CA 94035
2	Director US Army Research and Tech Laboratories (AVRADCOM) Ames Research Center Moffett Field, CA 94035
1	Commander US Army Communications Rsch and Development Command ATTN: DRDCO-PPA-SA Fort Monmouth, NJ 07703
1	Commander US Army Electronics Research and Development Command Technical Support Activity ATTN: DELSD-L Fort Monmouth, NJ 07703
1	Commander US Army Harry Diamond Labs 2800 Powder Mill Road Adelphi, MD 20783
1	Commander US Army Missile Command ATTN: DRSMI-R Redstone Arsenal, AL 35809
1	Commander US Army Missile Command ATTN: DRSMI-RBL Redstone Arsenal, AL 35809
1	Commander US Army Missile Command ATTN: DRSMI-YDL Redstone Arsenal, AL 35809
2	Commander US Army Mobility Equipment Research & Development Cmd Fort Belvoir, VA 22060

DISTRIBUTION LIST

No. of Copies	Organization
1	Commander US Army Tank Automotive Rsch and Development Command ATTN: DRDTA-UL Warren, MI 48090
2	Project Manager Tank Main Armament Systems ATTN: DRCPM-TMA Dover, NJ 07801
1	Product Manager for 30mm Ammo ATTN: DRCPM-AAH-30mm Dover, NJ 07801
2	Product Manager M110E2 Weapon System, DARCOM ATTN: DRCPM-M110E2 Rock Island, IL 61299
2	Project Manager Nuclear Munitions ATTN: DRCPM-NUC Dover, NJ 07801
2	Project Manager Cannon Artillery Weapons Systems ATTN: DRCPM-CAWS Dover, NJ 07801
2	Project Manager Division Air Defense Gun ATTN: DRCPM-ADG Dover, NJ 07801
4	Director US Army Materials and Mechanics Research Center ATTN: Director (3 cys) DRXMR-ATL Watertown, MA 02172
3	Commander US Army Research Office ATTN: Technical Director Engineering Division Metallurgy & Materials Div P. O. Box 12211 Research Triangle Park, NC 27709
2	Director US Army TRADOC Systems Analysis Activity ATTN: ATAA-SL, Tech Lib White Sands Missile Range NM 88002
1	Commander Naval Air Systems Command Washington, DC 20360
1	Commander Naval Sea Systems Command Washington, DC 20362
1	Commander Naval Air Development Center, Johnsville Warminster, PA 18974
1	Commander Naval Missile Center Point Mugu, CA 95041
2	Commander Naval Ship Research and Development Command Bethesda, MD 20084
2	Commander Naval Surface Weapons Center Dahlgren, VA 22448
2	Commander Naval Surface Weapons Center Silver Spring, MD 20910
2	Commander Naval Weapons Center China Lake, CA 93555
1	Commander Naval Research Laboratory Washington, DC 20375
1	Superintendent Naval Postgraduate School ATTN: Dir of Lib Monterey, CA 93940

DISTRIBUTION LIST

No. of Copies	Organization
1	Commander Naval Ordnance Station Indian Head, MD 20640
2	AFATL Eglin AFB, FL 32542
2	AFWL/SUL Kirtland AFB, NM 87117
2	ASD Wright-Patterson AFB, OH 45433
1	Director Lawrence Livermore Laboratory Livermore, CA 94550
1	Director Los Alamos Scientific Laboratory Los Alamos, NM 87544
1	Headquarters National Aeronautics and Space Administration Washington, DC 20546
2	Director National Aeronautics and Space Administration Langley Research Center Langley Station Hampton, VA 23365
1	Director National Aeronautics and Space Administration Manned Spacecraft Center ATTN: Lib Houston, TX 77058

Aberdeen Proving Ground

Dir, USAMSAA
ATTN: DRXSY-D
DRXSY-MP, H. Cohen
Cdr, USATECOM
ATTN: DRSTE-TO-F
Dir, USACSL, Bldg. E3516, EA
ATTN: DRDAR-CLB-PA
DRDAR-CL
DRDAR-CLD
DRDAR-CLB
DRDAR-CLY
DRDAR-CLN

END

DATE

FILMED

11-81

DTIC